jmb Article

Specific Domains of Aβ Facilitate Aggregation on and Association with Lipid Bilayers

Elizabeth A. Yates[1], Sherry L. Owens[1], Michael F. Lynch[1], Elena M. Cucco[2], C. Samuel Umbaugh[1] and Justin Legleiter[1,2,3]

1 - The C. Eugene Bennett Department of Chemistry, 217 Clark Hall, West Virginia University, Morgantown, WV 26506, USA
2 - Center for Neuroscience, Robert C. Byrd Health Sciences Center, PO Box 9304, West Virginia University, Morgantown, WV 26506, USA
3 - NanoSAFE, PO Box 6223, West Virginia University, Morgantown, WV 26506, USA

Correspondence to Justin Legleiter: *The C. Eugene Bennett Department of Chemistry, 217 Clark Hall, West Virginia University, Morgantown, WV 26506, USA. justin.legleiter@mail.wvu.edu*
http://dx.doi.org/10.1016/j.jmb.2013.03.022
Edited by R. Wetzel

Abstract

A hallmark of Alzheimer's disease, a late-onset neurodegenerative disease, is the deposition of neuritic amyloid plaques composed of aggregated forms of the β-amyloid peptide (Aβ). Aβ forms a variety of nanoscale, toxic aggregate species ranging from small oligomers to fibrils. Aβ and many of its aggregate forms strongly interact with lipid membranes, which may represent an important step in several toxic mechanisms. Understanding the role that specific regions of Aβ play in regulating its aggregation and interaction with lipid membranes may provide insights into the fundamental interaction between Aβ and cellular surfaces. We investigated the interaction and aggregation of several Aβ fragments ($Aβ_{1–11}$, $Aβ_{1–28}$, $Aβ_{10–26}$, $Aβ_{12–24}$, $Aβ_{16–22}$, $Aβ_{22–35}$, and $Aβ_{1–40}$) in the presence of supported model total brain lipid extract (TBLE) bilayers. These fragments represent a variety of chemically unique domains within Aβ, that is, the extracellular domain, the central hydrophobic core, and the transmembrane domain. Using scanning probe techniques, we elucidated aggregate morphologies for these different Aβ fragments in free solution and in the presence of TBLE bilayers. These fragments formed a variety of oligomeric and fibrillar aggregates under free solution conditions. Exposure to TBLE bilayers resulted in distinct aggregate morphologies compared to free solution and changes in bilayer stability dependent on the Aβ sequence. $Aβ_{10–26}$, $Aβ_{16–22}$, $Aβ_{22–35}$, and $Aβ_{1–40}$ aggregated into a variety of distinct fibrillar aggregates and disrupted the bilayer structure, resulting in altered mechanical properties of the bilayer. $Aβ_{1–11}$, $Aβ_{1–28}$, and $Aβ_{12–24}$ had minimal interaction with lipid membranes, forming only sparse oligomers.

Introduction

Conformational or 'protein misfolding' diseases are defined by the rearrangement of specific proteins to non-native conformations, promoting the formation and deposition of toxic, nanoscale aggregates within tissues or cellular compartments. A pathological hallmark of Alzheimer's disease (AD), an age-related neurodegenerative disease, is the formation of neuritic amyloid plaques. These plaques consist predominantly of extracellular masses of filamentous aggregates of the β-amyloid peptide (Aβ) as well as other plaque-associated proteins (e.g., apoE, apoJ, inflammatory molecules), which are associated with dystrophic dendrites and axons, activated microglia, and reactive astrocytes.[1] Aβ is a monomeric, amphipathic, 39- to 43-amino-acid residue cleavage product of the transmembrane amyloid precursor protein.[2]

Like many other amyloid-forming peptides, Aβ can form a variety of aggregate structures on and off pathway to fibril formation, including distinct oligomers and protofibrils.[2,3] Beyond this heterogeneity of smaller intermediate aggregate structures, Aβ also has the ability to form numerous morphologically distinct fibril structures, often referred to as polymorphs.[4–7] A variety of environmental factors can influence the emergence of different polymorphic

fibrils. For example, varying sample preparation of $A\beta_{1-40}$ results in five structurally distinct fibrillar aggregates *in vitro*.[6] Furthermore, Aβ can bind metal ions, and their presence in solution can facilitate aggregation leading to neurotoxicity.[8–10] As such, several small molecules that inhibit metal-induced Aβ aggregation for potential therapeutic purposes have been developed.[11–13] Another contributing factor to the emergence of distinct polymorphic aggregates is the presence of surfaces. Aβ aggregates into distinct forms in the presence of mica and graphite.[14–16] The addition of disease-related point mutations can directly lead to distinct polymorphic aggregates of Aβ in the presence of surfaces,[17] suggesting that electrostatic and hydrophobic interactions between the peptide and surface strongly influence the aggregation process. The role of surfaces may underlie the ability of different synthetic nanoparticles, which have high surface-to-volume ratios, to either promote[18] or inhibit[19] Aβ aggregation, and thus could prove useful in understanding their potential therapeutic use. The formation of specific polymorphs may play an important role in disease pathology, as two structurally distinct polymorphic fibrils of $A\beta_{1-40}$ were associated with significantly different levels of toxicity to neuronal cell cultures.[20]

With respect to surfaces, a potentially relevant environmental factor regulating Aβ aggregation is lipid bilayers. The fluid surfaces provided by lipid bilayers are well known to influence protein structure and dynamics, which can nucleate the aggregation process. Importantly for AD, lipid bilayer properties alter protein conformation and exert enormous influence on the aggregation state, as substantial enhancement of Aβ aggregation is observed in the presence of lipid membranes.[21–25] While cellular membranes may act to aid protein aggregation,[26–28] these same membranes may be damaged by the aggregation process, leading to membrane dysfunction caused by membrane permeabilization by Aβ either perturbing bilayer structure[29,30] or forming unregulated pores.[31–34] While several physicochemical aspects of membranes (such as phase state, curvature, charge, and elasticity) associated with lipid composition play an important role in specific peptide/lipid interactions, these interactions are also dependent on protein properties. Understanding the basic interaction between Aβ and lipid membranes could lead to a better understanding of Aβ aggregation associated with cellular membranes.

As Aβ is a cleavage product of amyloid precursor protein, it contains a hydrophobic transmembrane domain and a predominately hydrophilic extracellular domain, imparting amphiphilic character to Aβ (Fig. 1). Furthermore, based on a variety of structural and computational studies, several domains have been identified in Aβ. The N-terminal region of Aβ has been shown to form α-helical or β-sheet

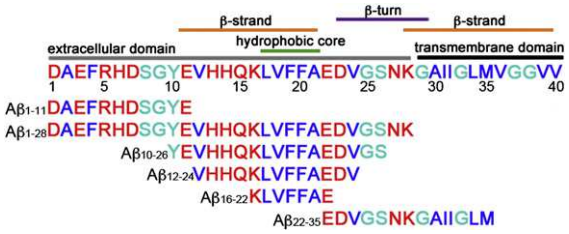

Fig. 1. Schematic representation of Aβ and specific domains. Using the hydropathy index, each sequence has hydrophilic (red), hydrophobic (blue), and slightly hydrophobic (light blue) amino acids. The aggregation of $A\beta_{1-11}$, $A\beta_{1-28}$, $A\beta_{10-26}$, $A\beta_{12-24}$, $A\beta_{16-22}$, $A\beta_{22-35}$, and $A\beta_{1-40}$ was investigated here.

structure dependent on solution conditions, such as pH.[35,36] The hydrophobic C-terminal end of Aβ has a high propensity to aggregate into β-sheet-rich structures independent of solvent conditions.[35,36] Despite the appearance of various polymorphs, Aβ fibrils are composed of bundled β-sheets with backbones orthogonal to the fiber axis creating a cross-β structure.[37] Site-directed spin labeling electron paramagnetic resonance studies of Aβ fibrils identified two β-strand-forming domains (residues 11–21 and 29–39, respectively) separated by turn/bend region (around residues 23–26).[38] NMR studies on a variety of Aβ fragments support the notion of two β-strand regions separated by a β-turn in different fibril structures.[20,39,40] The appearance of a β-turn between two β-strands is further supported by computational studies of Aβ fibrils.[41] The central region of Aβ (residues 16–21) has been shown to form a hydrophobic core with enhanced amyloidogenic properties[42] and is contained within one of the β-strand-forming regions. A variety of NMR studies of Aβ in solution indicate that the monomer is predominately unstructured with fluctuating residual structure.[43,44] A more recent NMR study though has demonstrated that this central hydrophobic domain of Aβ can form a 3_{10} helix, resulting in a compact structure as other hydrophobic residues cluster against the helix.[45] The variations in Aβ monomer and aggregate structure associated with these different studies may be partially attributed to the variation in preparation protocols that lead to polymorphic aggregates.

Here, we sought to determine the role specific domains of Aβ play in its aggregation under free solution conditions and in the presence of total brain lipid extract (TBLE) bilayers. The aggregation of seven different Aβ fragments ($A\beta_{1-11}$, $A\beta_{1-28}$, $A\beta_{10-26}$, $A\beta_{12-24}$, $A\beta_{16-22}$, $A\beta_{22-35}$, and $A\beta_{1-40}$) was investigated. These Aβ fragments represent a variety of chemically unique regions, that is, the extracellular domain, the central hydrophobic core, different β-strand-forming sequences, and the trans-

membrane domain (Fig. 1). Atomic force microscopy (AFM) was used to characterize the Aβ fragment aggregate morphology and to monitor the degree of interaction with a model lipid bilayer system. In addition, we determined the mechanical impact of exposure to the different Aβ fragments on the TBLE bilayers.

Results

Aβ fragments form distinct oligomeric and fibrillar aggregates in free solution

To compare oligomers and fibrils formed by different Aβ fragments under free solution conditions (i.e., no surface present), we incubated 20-μM solutions of $Aβ_{1–11}$, $Aβ_{1–28}$, $Aβ_{10–26}$, $Aβ_{12–24}$, $Aβ_{16–22}$, $Aβ_{22–35}$, or $Aβ_{1–40}$ at 37 °C and sampled them at different time points, deposited them on mica, and imaged them by AFM in air. Each Aβ fragment was prepared via the same protocol[46] to ensure that observed differences in aggregate morphology were not attributable to sample preparation, which has been shown to profoundly influence Aβ aggregate morphology.[6] Each fragment was capable of forming discrete, globular oligomers within an hour of incubation (Fig. 2a). These oligomers were present for the entire length of the incubation (up to 72 h), although the relative abundance decreases when fibrils appeared for each respective fragment. Oligomers were defined as having an aspect ratio (longest distance across to shortest distance across) of less than 2, indicating a round, globular structure, allowing us to distinguish them from fibrils and other aggregates via image processing software. A summary of the number of replicates, images, and time points used in the following analysis is presented in Supplemental Table 1.

Height analysis of oligomers suggested that the Aβ fragments formed different oligomeric species (Fig. 2b). The height of an individual oligomer was defined as the largest height value (pixel in the image) contained within the globular structure constituting one oligomer in the AFM image. While one could predict that the height of oligomers would correlate with the size of the individual fragments, this was not necessarily the case. $Aβ_{1–40}$, being the largest fragment, did form the largest oligomers (average height of 7.8 ± 3.5 nm and a mode of ~5–8 nm). Fragments that predominately contained the extracellular domain aggregated into the smallest oligomers with $Aβ_{1–11}$ and $Aβ_{1–28}$ having average oligomer heights of 3.8 ± 3.3 nm and 3.3 ± 1.9 nm, respectively. Due to the distribution of oligomer height being skewed toward larger values for both $Aβ_{1–11}$ and $Aβ_{1–28}$, the modes of the height were smaller (0.5–1.5 nm for $Aβ_{1–11}$ and 2–3 nm for $Aβ_{1–28}$). The relatively small height was observed despite $Aβ_{1–28}$ being the second largest fragment studied. $Aβ_{1–11}$ aggregated into a more heterogeneous population of oligomers compared to $Aβ_{1–28}$. Two of the three fragments containing the central hydrophobic/amyloidogenic core of Aβ ($Aβ_{10–26}$ and $Aβ_{12–24}$) formed similar sized oligomers, suggesting that the core region may organize to form specific oligomeric species. $Aβ_{16–22}$, being a much smaller fragment, formed a smaller oligomer. The height of oligomers for these three fragments were 4.1 ± 2.5 nm for $Aβ_{10–26}$, 4.2 ± 2.4 nm for $Aβ_{12–24}$, and 2.9 ± 1.1 nm for $Aβ_{16–22}$. The modes of oligomer height composed of $Aβ_{10–26}$ or $Aβ_{12–24}$ were 3–4 nm, and it was 2–3 nm for $Aβ_{16–22}$. $Aβ_{22–35,}$ which does not contain the amyloid core region but does have a portion of the transmembrane domain, formed smaller (average height of 2.5 ± 1.0 nm and a mode of 2–3 nm) oligomers with a very tight distribution compared to the other fragments.

To further characterize the size of oligomers formed by the different Aβ fragments, we used volume distributions of individual oligomers (obtained via an aspect ratio filter) to estimate the approximate molecular weight of oligomers. As the measured volume of each oligomer is exaggerated due to the size and shape of the AFM tip, a partial correction based on geometric models was applied to the volumes observed for individual oligomers.[47] The volume of individual oligomers was converted to an approximate molecular weight based on the average density of proteins.[48,49] Following this protocol, molecular weight distributions of oligomers formed by each fragment were obtained (Fig. 2c). Unsurprisingly, $Aβ_{1–40}$ formed the largest oligomers with a broad distribution. Aβ fragments that contained the extracellular domain formed the smallest oligomers, although oligomers of $Aβ_{1–11}$ were smaller (~20 kDa) than those formed by $Aβ_{1–28}$ (~40–60 kDa). The oligomers formed by $Aβ_{10–26}$, $Aβ_{12–24}$, or $Aβ_{16–22}$ (the three fragments that contained the hydrophobic core) systematically decreased in mass in a manner consistent with the size of each respective monomer (~125–150 kDa for $Aβ_{10–26}$, ~90–120 kDa for $Aβ_{12–24}$, and ~75–100 kDa for $Aβ_{16–22}$). This suggests that these oligomers are composed of a similar number of peptides. As the common sequence between these three fragments was the hydrophobic core, it is likely that this sequence is driving the formation of oligomers of these three fragments. $Aβ_{22–35}$ aggregated into smaller oligomeric structures (~70–80 kDa) compared to fragments containing the hydrophobic core, but larger than those formed by fragments containing the extracellular domain.

All of the Aβ fragments aggregated into fibrils (Fig. 3a); however, the time needed to observe fibrils and their morphology was fragment specific. $Aβ_{1–40}$

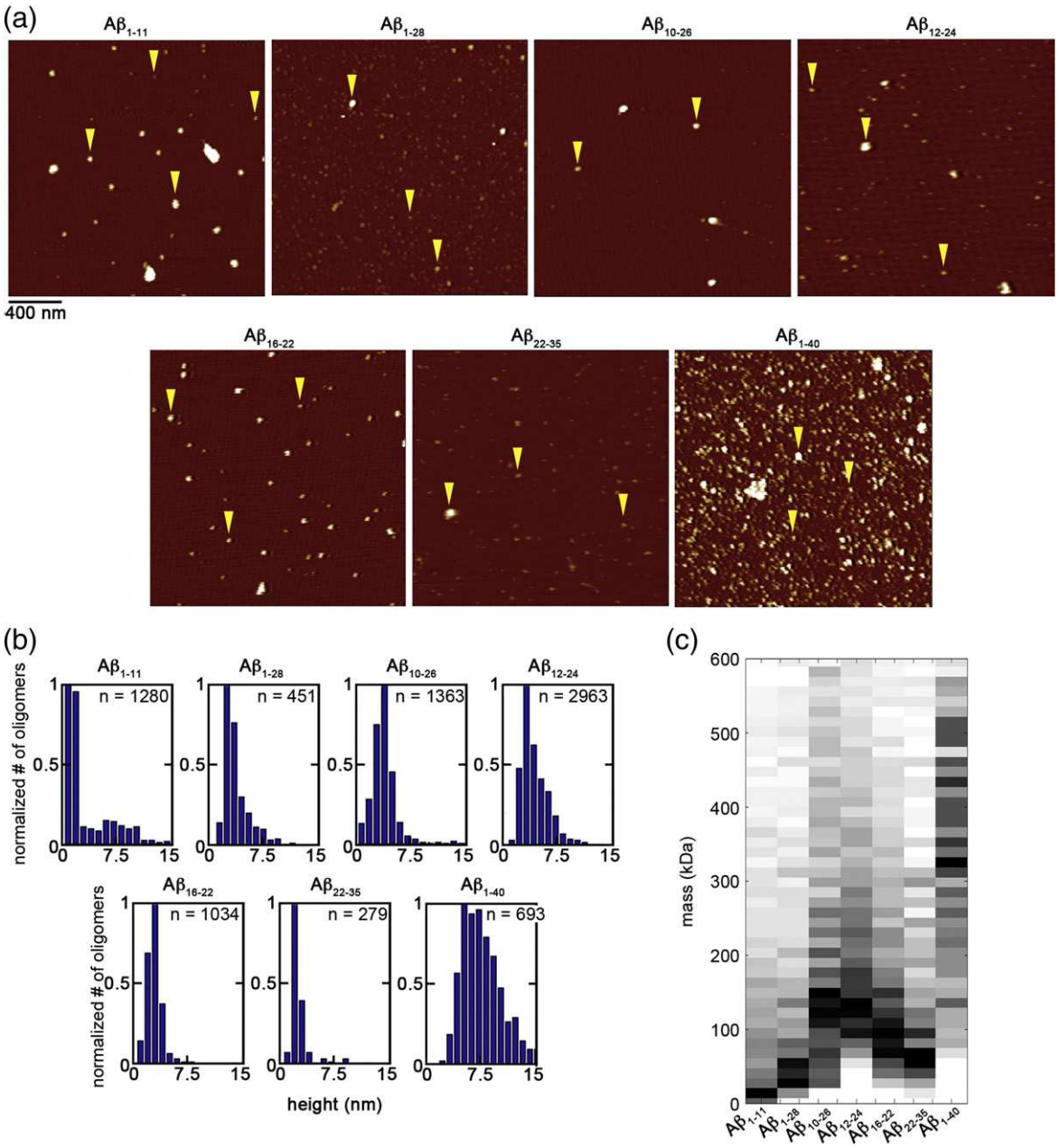

Fig. 2. Aβ fragments form oligomers under free solution conditions. Oligomers formed by $Aβ_{1–11}$, $Aβ_{1–28}$, $Aβ_{10–26}$, $Aβ_{12–24}$, $Aβ_{16–22}$, $Aβ_{22–35}$, and $Aβ_{1–40}$ formed a variety of oligomers. (a) Representative AFM images of oligomeric aggregates formed by different Aβ fragments. The scale bar is applicable to all images. Representative oligomers are indicated by yellow arrows. (b) Height histograms for oligomers formed by the different Aβ fragments. The total number (*n*) of measured oligomers used to construct each histogram is indicated for each fragment. The histograms were compiled from a minimum of six images taken from at least three independent experiments. (c) Based on corrected volume measurements, the molecular mass of oligomers formed by each Aβ fragment was calculated. The darker colors represent a greater population of oligomers at that molecular mass.

aggregated into fibrils within 24 h of incubation. The $Aβ_{1–11}$ took 72 h of incubation for fibrils to appear, and this extended incubation time needed for fibril formation was most likely due to the lack of a β-strand region within this fragment. Fibrils were observed for the other fragment predominately composed of the extracellular domain, $Aβ_{1–28}$, within 48 h. The shorter time of fibril formation for $Aβ_{1–28}$ in comparison with $Aβ_{1–11}$ was most likely aided by the inclusion of a β-strand region in the longer fragment. $Aβ_{10–26}$, $Aβ_{12–24}$, and $Aβ_{16–22}$, despite aggregating into similar sized oligomers, assembled into fibrils

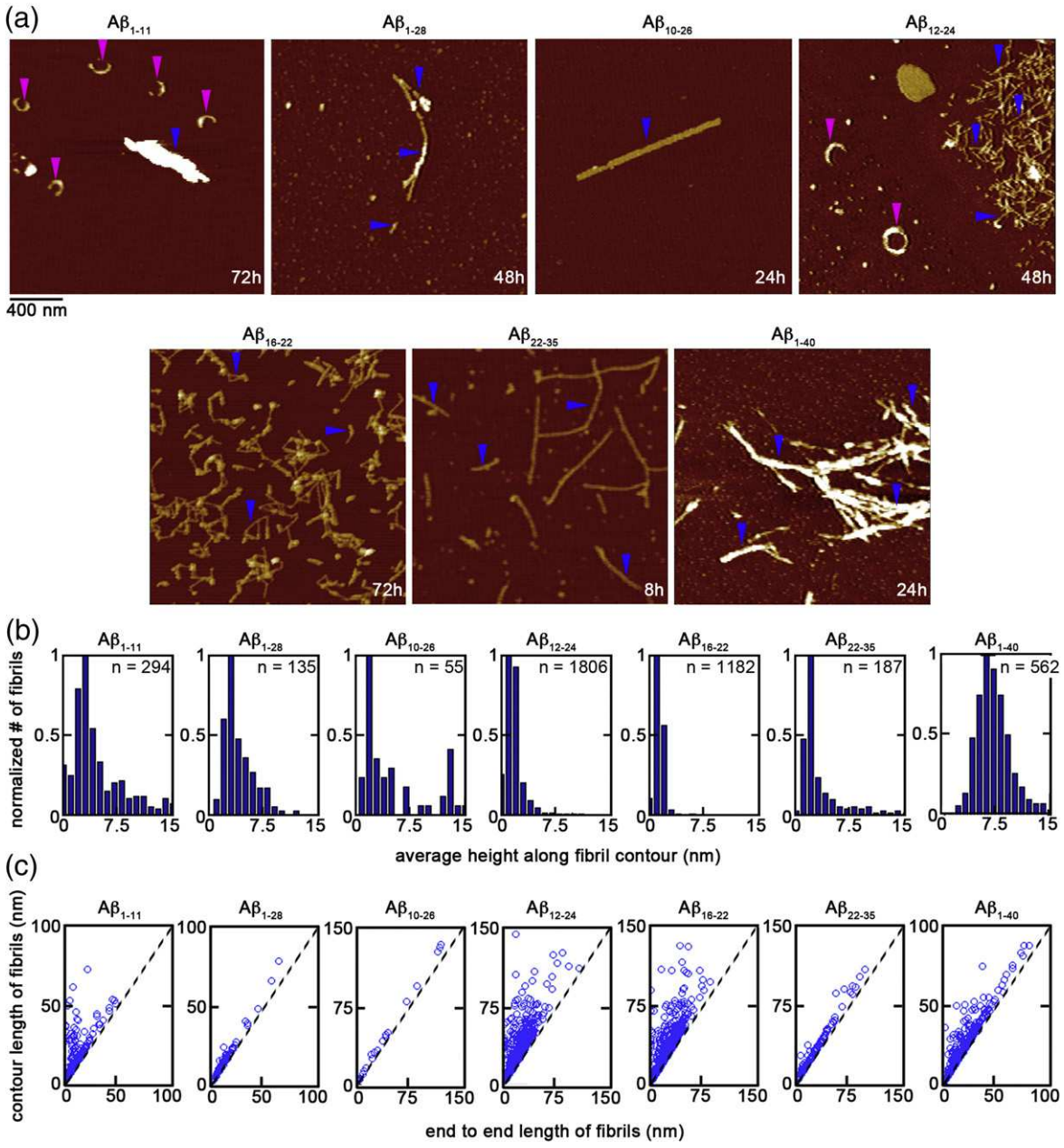

Fig. 3. Aβ fragments form fibrils in free solution with distinct morphologies. (a) Representative *ex situ* AFM images of fibrils composed of $A\beta_{1-11}$, $A\beta_{1-28}$, $A\beta_{10-26}$, $A\beta_{12-24}$, $A\beta_{16-22}$, $A\beta_{22-35}$, or $A\beta_{1-40}$. The images were taken at the time points when fibrils were first observed to form, as indicated. The scale bar is applicable to all images. Arrows indicate annular aggregates (pink) and fibrils (blue). (b) Histograms of the average height along the contour of the fibril for fibrils formed by each Aβ fragment are presented. The total number (*n*) of measured fibrils used to construct each histogram is indicated for each fragment. The histograms were compiled from a minimum of three images taken from at least three independent experiments. (c) Plots correlating the contour length to the end-to-end distance of fibrils formed from the different Aβ fragments are shown. The broken lines represent the theoretical correlation for rigid rod-like structures with infinite persistence lengths.

after approximately 24 h, 48 h, and 72 h of incubation. The time required for these three fragments containing the hydrophobic core of Aβ to aggregate into fibrils roughly correlated with the length of the fragment, with fibrils appearing earlier for longer fragments. For these three fragments ($A\beta_{10-26}$, $A\beta_{12-24}$, and $A\beta_{16-22}$), the longer sequences have more sites where β-sheet formation can nucleate, leading to earlier fibril formation. Fibrils of $A\beta_{22-35}$ formed most quickly, within 8 h of incubation. The

formation of $A\beta_{22–35}$ fibrils was likely facilitated by the β-strand-forming sequence associated with the transmembrane domain and the tight distribution of oligomers that may be on pathway to fibril formation. The relatively quick formation of fibrils for $A\beta_{22–35}$ and $A\beta_{1–40}$, both of which contain at least a portion of the transmembrane domain, indicates that the transmembrane portion of Aβ plays an important role in nucleating fibril formation.

It is important to note, however, that the morphology of the fibrils formed by the different fragments varied (Fig. 3a). As a result, we performed a variety of image analyses to investigate these morphological differences. The average height (or thickness perpendicular to the long axis of the fibril) along the entire contour of each fibril was determined because height can vary along the extended morphology of a fibril (note: this is a different method of determining the height than was used for analysis of oligomers). This average height along the contour varied for fibrils composed of the different Aβ fragments (Fig. 3b). As expected, $A\beta_{1–40}$ formed the thickest

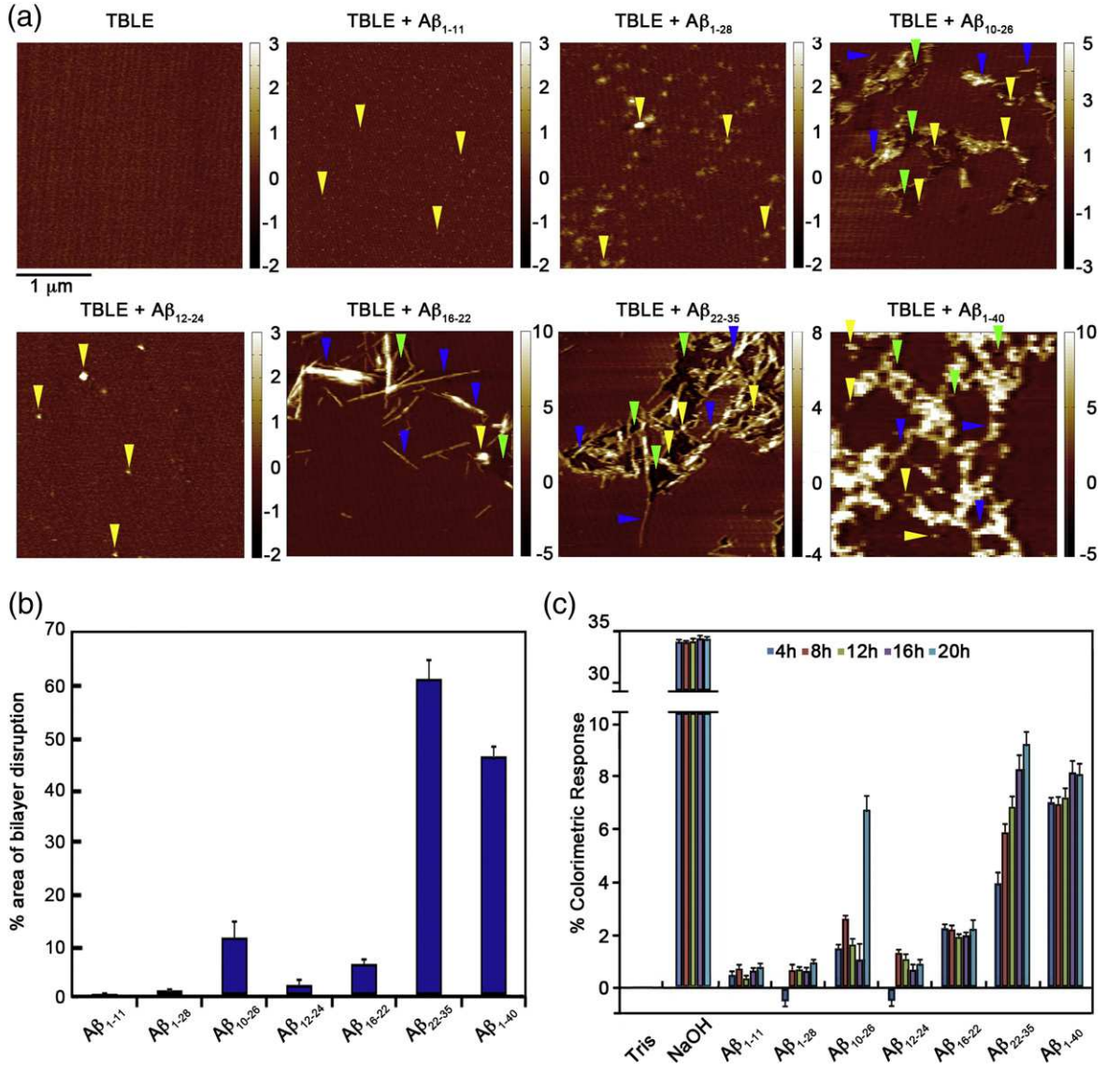

Fig. 4. Aβ fragments have varying levels of interaction with lipid membranes. (a) Representative *in situ* AFM images of TBLE bilayers exposed to $A\beta_{1–11}$, $A\beta_{1–28}$, $A\beta_{10–26}$, $A\beta_{12–24}$, $A\beta_{16–22}$, $A\beta_{22–35}$, or $A\beta_{1–40}$ for 16–20 h. The scale bar is applicable to all images. Arrows indicate oligomers (yellow), fibrils (blue), and areas of exposed mica (green). (b) Percent area of the TBLE bilayer surface occupied by Aβ fragment aggregates or increased bilayer disruption was measured from images obtained after 16–20 h of bilayer exposure to different Aβ fragments. (c) The percent colorimetric response (%CR) of TBLE/PDA vesicles exposed to different Aβ fragments as a function of time is presented. Exposure to Tris and NaOH acted as negative and positive controls, respectively. %CR values were averaged over three samples.

fibrils (average height of 7.3 ± 2.4 nm and a mode of ~5–8 nm) with a highly entangled morphology. Unlike the case with oligomers, fragments containing the extracellular domain formed intermediate sized fibrils with $A\beta_{1-11}$ and $A\beta_{1-28}$ having average fibril heights of 3.5 ± 2.3 nm and 3.2 ± 1.9 nm along the fibril contour, respectively. The three fragments containing the hydrophobic core formed very similar sized fibrils (1.5 ± 2.5 nm for $A\beta_{10-26}$, 1.2 ± 2.4 nm for $A\beta_{12-24}$, and 1.9 ± 1.1 nm for $A\beta_{16-22}$) that were smaller than fibrils formed by other fragments. The similarity between these average heights along the fibril contour suggests that the hydrophobic core is dictating the fibril structure. The mode of fibril heights composed of $A\beta_{10-26}$ was ~1–2 nm, and the mode was ~0.5–1.5 for fibrils of both $A\beta_{12-24}$ and $A\beta_{16-22}$. It should also be noted that of these three fragments, only $A\beta_{12-24}$ formed a subpopulation of annular aggregates. $A\beta_{22-35}$ formed slightly thicker fibrils compared to those containing the hydrophobic core (average height of 2.5 ± 1.0 nm and a mode of 2–3 nm).

The fibrils formed by the different fragments displayed varying amounts of curvature (or persistence length) along their long axis. In an effort to more clearly demonstrate this feature, the relationship between the contour length and end-to-end distance was compared (Fig. 3c). Rigid structures that have an infinitely large persistence length would have equal contour lengths and end-to-end distances. Such a scenario would result in a correlation plot with a slope of 1 (represented by the broken line seen in each correlation plot in Fig. 3c). Deviations from this theoretical broken line indicated that the fibril structure has a smaller persistence length, and the further the deviation, the lower the persistence length. Trends in the relative rigidity of the fibril structure along its long axis can be seen based on the specific domains contained in each fragment. Based on these correlation plots, $A\beta_{1-11}$ formed a large population of highly curved fibrillar aggregates, which can be seen as half ring-like structures in the corresponding AFM image (Fig. 3a). This ability to form highly curved fibrils of $A\beta_{1-11}$ may be due to the lack of any known β-strand-forming domains within this fragment. In comparison, $A\beta_{1-28}$ and $A\beta_{10-26}$ formed fibril structures with relatively large persistence lengths, both of which contain a large portion of the first β-strand-forming domain in Aβ. $A\beta_{22-35}$, which contained a portion of the second β-strand-forming domain, also formed fibrils with large persistence lengths. Reducing the size of the β-strand-forming domain appeared to reduce the persistence length of the fibrils, as $A\beta_{12-24}$ and $A\beta_{16-22}$ aggregated into highly curved fibrils that deviated from the theoretical rigid line in the correlation plot between contour length and end-to-end distance (Fig. 3c). $A\beta_{1-40}$, despite containing both β-strand-forming domains, aggregated into fibrils that had intermediate persistence lengths.

Aβ fragments form distinct aggregates in the presence of supported bilayers

To investigate the interaction between specific Aβ fragments and lipid membranes, we exposed supported TBLE bilayers to each fragment and imaged them using *in situ* AFM. TBLE bilayers contain a physiologically relevant mix of lipid components, that is, cholesterol, gangliosides, sphingolipids, isoprenoids, and both acidic and neutral phospholipids, making these bilayers an appropriate model surface. Defect-free bilayers (as determined by AFM) were produced via vesicle fusion, and such supported lipid bilayers have been shown to maintain many properties of free membranes.[50,51] The defect-free TBLE bilayers were stable for at least 24 h and had an RMS surface roughness of 0.21 ± 0.07 nm.

TBLE bilayers were exposed to 20-μM (final concentration) solutions of each Aβ fragment ($A\beta_{1-11}$, $A\beta_{1-28}$, $A\beta_{10-26}$, $A\beta_{12-24}$, $A\beta_{16-22}$, $A\beta_{22-35}$, or $A\beta_{1-40}$) at ~21–22 °C (Fig. 4a) by direct injection of the peptides into the AFM fluid cell. As continual imaging by the AFM tip was found to interfere with the interaction of some of the Aβ fragments with the bilayer, an image was taken directly after injection to ensure no damage to the bilayer due to the injection process, and then the imaging process was stopped. After 16 h of co-incubation, AFM imaging was resumed; therefore, all presented AFM images were taken between 16 and 20 h after the injection of peptide (Fig. 4a). A summary of the number of replicates, images, and time points used in the following analysis is presented in Supplemental Table 1. As has been previously observed in the literature,[24,25] $A\beta_{1-40}$ readily aggregated into fibrils and oligomers on the TBLE bilayer, creating regions of increased surface roughness (RMS roughness of 6.9 ± 0.5 nm) that can be associated with disruption of lipid packing within the bilayer. The large surface roughness is partially due to a combination of the large size of aggregates associated with these regions and holes that span the entire bilayer. For Aβ sequences predominately containing the extracellular domain ($A\beta_{1-11}$ and $A\beta_{1-28}$), a small number of oligomers appeared on the TBLE bilayer, with no discernible effect on the bilayer integrity or roughness. Presumably, the hydrophilic nature of the extracellular domain does not provide an adequate driving force for substantial association between Aβ and the lipid bilayer. Of the peptides containing the hydrophobic core, $A\beta_{12-24}$ only formed oligomeric aggregates on the bilayer, resulting in limited changes in the bilayer's stability and morphology. However, $A\beta_{10-26}$ and $A\beta_{16-22}$ both extensively aggregated into oligomers and fibrils in the presence of the bilayer, and these aggregates were

often associated with regions of the TBLE bilayer displaying increased surface roughness (~1.6 ± 0.1 nm for $A\beta_{10-26}$ and ~5.9 ± 0.5 nm for $A\beta_{16-22}$) or holes spanning the entire membrane. $A\beta_{22-35}$ aggregated predominately into fibrils (with some oligomers present) and aggressively disrupted the TBLE bilayer (RMS roughness ~3.8 ± 0.2 nm) to expose large areas of mica, suggesting that the transmembrane domain mediates the interaction between Aβ and lipid bilayers. As both mica (Supplemental Fig. 1) and unperturbed TBLE bilayers (Fig. 4a) appear smooth in AFM images, the creation of holes in the bilayer that exposed the underlying mica substrate was evident by ~4- to 5-nm step features in the AFM images (Fig. 4a).

The extent of interaction of the different fragments with the bilayer was determined by calculating the percent surface area that contained aggregates or increased surface roughness (Fig. 4b). Based on this analysis, the fragments that contained a portion of the transmembrane domain ($A\beta_{22-35}$ and $A\beta_{1-40}$) had the strongest interaction with the TBLE bilayer as at least half of the available bilayer surface was typically disrupted after 16 h of exposure. Peptides that contained the hydrophobic core typically disrupted 5–15% of the surface, with $A\beta_{10-26}$ being the most aggressive of these three fragments. $A\beta_{1-11}$ and $A\beta_{1-28}$ minimally interacted with the TBLE bilayer, as only a small fraction of the surface was occupied by discrete oligomers.

To verify the observed magnitude of the interaction of the different Aβ fragments with the TBLE bilayers as measured by *in situ* AFM and gain some time-resolved information about this interaction, we

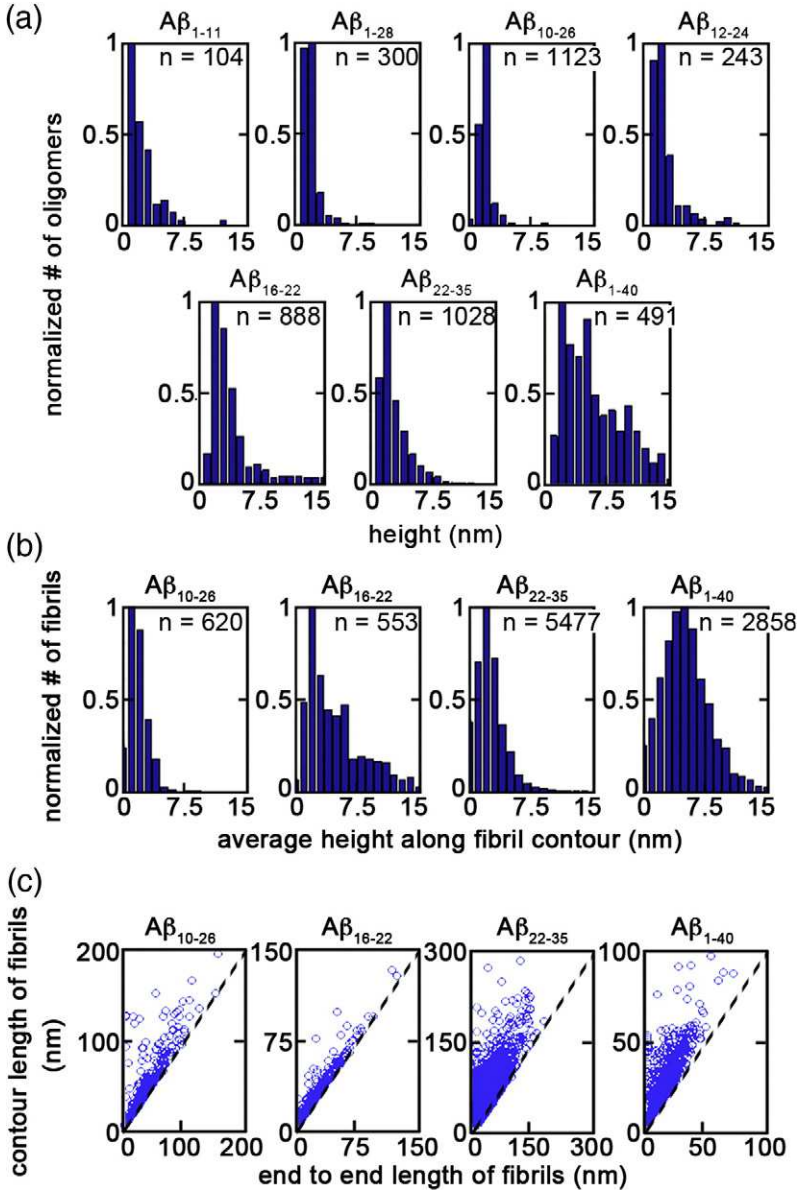

Fig. 5. Aβ fragments form a variety of oligomers and fibrils on TBLE bilayers. (a) Height histograms of oligomers formed by $A\beta_{1-11}$, $A\beta_{1-28}$, $A\beta_{10-26}$, $A\beta_{12-24}$, $A\beta_{16-22}$, $A\beta_{22-35}$, or $A\beta_{1-40}$ in the presence of TBLE bilayers are shown. (b) Histograms of the average height along the contour of the fibril for fibrils formed by each $A\beta_{10-26}$, $A\beta_{16-22}$, $A\beta_{22-35}$, or $A\beta_{1-40}$ in the presence of TBLE bilayers are presented. The total number (*n*) of measured oligomers and fibrils used to construct each histogram is indicated for each fragment. The histograms were compiled from a minimum of six images taken from at least three independent experiments. (c) Plots correlating the contour length to the end-to-end distance of fibrils formed from $A\beta_{10-26}$, $A\beta_{16-22}$, $A\beta_{22-35}$, or $A\beta_{1-40}$ in the presence of TBLE bilayers are shown. The broken lines represent the theoretical correlation for rigid rod-like structures with infinite persistence lengths.

performed a series of colorimetric membrane binding assays using lipid/polydiacetylene (PDA) vesicles. Lipid/PDA vesicles have varied colorimetric responses (CRs) when exposed to proteins depending on the extent of the protein/lipid interaction.[52,53] The CR in the lipid/PDA vesicles is related to transitions of the PDA polymer backbone structure, which is affected by changes in tension associated with protein interaction with and/or insertion into the vesicle.[53] By measuring absorbance of both the blue (640 nm) and red (500 nm) wavelengths of TBLE/PDA vesicles upon exposure to different Aβ fragments, the percent CR was obtained, which directly corresponds to the protein/lipid interaction (Fig. 4c). Exposure to Tris or NaOH was used as negative and positive controls. NaOH acts as a positive control for vesicle perturbation because, as a strong base, it can decompose lipids, changing the tension in the vesicle and inducing a CR. These PDA/TBLE experiments correspond well with our AFM observations (the 16- and 20-h time points can be directly compared to Fig. 4b). $A\beta_{1-11}$ and $A\beta_{1-28}$ had induced the smallest CR. A larger CR was observed for the Aβ fragments containing the hydrophobic core, and the relative magnitude of this response was consistent with the AFM data. The largest CR was observed when the vesicles were exposed to $A\beta_{22-35}$ and $A\beta_{1-40}$, verifying that the transmembrane domain plays a key role in the interaction of Aβ with lipid membranes. Despite both invoking a large CR, there were differences in the time-dependent interaction of $A\beta_{22-35}$ and $A\beta_{1-40}$ with the PDA/TBLE vesicles. While $A\beta_{1-40}$ quickly interacted with the vesicles, the CR quickly leveled off. $A\beta_{22-35}$ did not initially invoke a large CR; however, the interaction with the vesicles steadily increased with time.

Next, we performed analysis of the aggregate morphologies observed for each Aβ fragment upon exposure to the TBLE bilayer via AFM image analysis (Fig. 5). Each Aβ fragment formed oligomers (aggregates with an aspect ratio less than 2) on the TBLE bilayer, and we analyzed the height of these oligomers (Fig. 5a). Small oligomers of $A\beta_{1-11}$ associated with the bilayer (mode ~ 0.5 nm; average height of 2.6 ± 2.4 nm) were similar in morphology to the smaller population of $A\beta_{1-11}$ oligomers that formed under free solution conditions; however, the population of larger oligomers that were observed in free solution was absent in the presence of the bilayer, suggesting that the bilayer either preferentially binds the smaller oligomers or promotes their formation. Oligomers of $A\beta_{1-28}$ were smaller in the presence of the TBLE bilayer (mode ~1–2 nm; average height of 1.8 ± 0.8 nm) compared to oligomers formed under free solution conditions, suggesting either that the bilayer promotes the formation of smaller oligomers or that the oligomers are partially inserted into the bilayer. The fragments that contained the hydrophobic core of Aβ formed smaller oligomers (mode ~0.5–2 nm for $A\beta_{10-26}$, 0.5–2 nm for $A\beta_{12-24}$, and 1.0–2.5 nm for $A\beta_{16-22}$) compared to those observed under free solution conditions. Again, a plausible explanation for this observation is that these oligomers are partially inserted into the bilayer. Due to the appearance of some larger oligomers, the average height of oligomers were larger than the mode for these three fragments (4.0 ± 1.9 nm for $A\beta_{10-26}$, 2.4 ± 1.7 nm for $A\beta_{12-24}$, and 4.6 ± 3.1 nm for $A\beta_{16-22}$). $A\beta_{22-35}$ oligomers were similar in size (mode ~1.0–2.5 nm) in the presence of the bilayer compared to their free solution counterparts, but the distribution was much broader with some larger oligomers being observed. $A\beta_{1-40}$ oligomers were on average smaller compared to those observed in free solution (5.2 ± 3.1 nm), also suggesting partial insertion into the bilayer. However, the distribution of sizes of $A\beta_{1-40}$ oligomers became much broader.

The appearance of fibrils on TBLE bilayers was only observed for $A\beta_{10-26}$, $A\beta_{16-22}$, $A\beta_{22-35}$, and $A\beta_{1-40}$, and these fibrils varied morphologically (Fig. 5b and c). The time frame for fibrils of these four fragments to form on the bilayer was reduced in comparison to free solution conditions, suggesting that the lipid environment facilitates the formation of fibrils for these specific fragments. As there was a limited time period for which we were able to observe the TBLE bilayers, we cannot rule out that $A\beta_{1-11}$, $A\beta_{1-28}$, and $A\beta_{12-24}$ would form fibrils on the bilayer given more time, especially considering that it took at least 48 h for fibrils to be observed for these three fragments under free solution conditions. Fibrils of $A\beta_{10-26}$ that formed on the bilayer were similar in height (1.8 ± 1.1 nm) (Fig. 5b) but appeared to have a smaller persistence length (Fig. 5c) compared to fibrils formed in free solution. Due to these characteristics and the appearance of the fibrils, it appeared that $A\beta_{10-26}$ aggregated into a distinct polymorphic fibril on the bilayer compared to those observed from free solution. $A\beta_{16-22}$ aggregated into a much longer, thicker (average height of 5.4 ± 2.4 nm), and rigid (high persistence length) fibrillar polymorph than was observed in free solution. $A\beta_{22-35}$ formed thicker (2.5 ± 1.9 nm) and more rigid fibrillar aggregates on the bilayer in comparison to free solution, and these fibrils were predominately associated with complete disruption of the membrane, exposing mica. Based on appearance, $A\beta_{1-40}$ formed a different fibril structure on the bilayer compared with free solution. The height of these $A\beta_{1-40}$ fibrils on the bilayer was slightly smaller (5.2 ± 3.1 nm) with higher curvature than their free solution counterparts.

Aβ fragments alter the local mechanical properties of TBLE bilayers

Next, we determined how exposure to the different Aβ fragments altered the local compressibility and

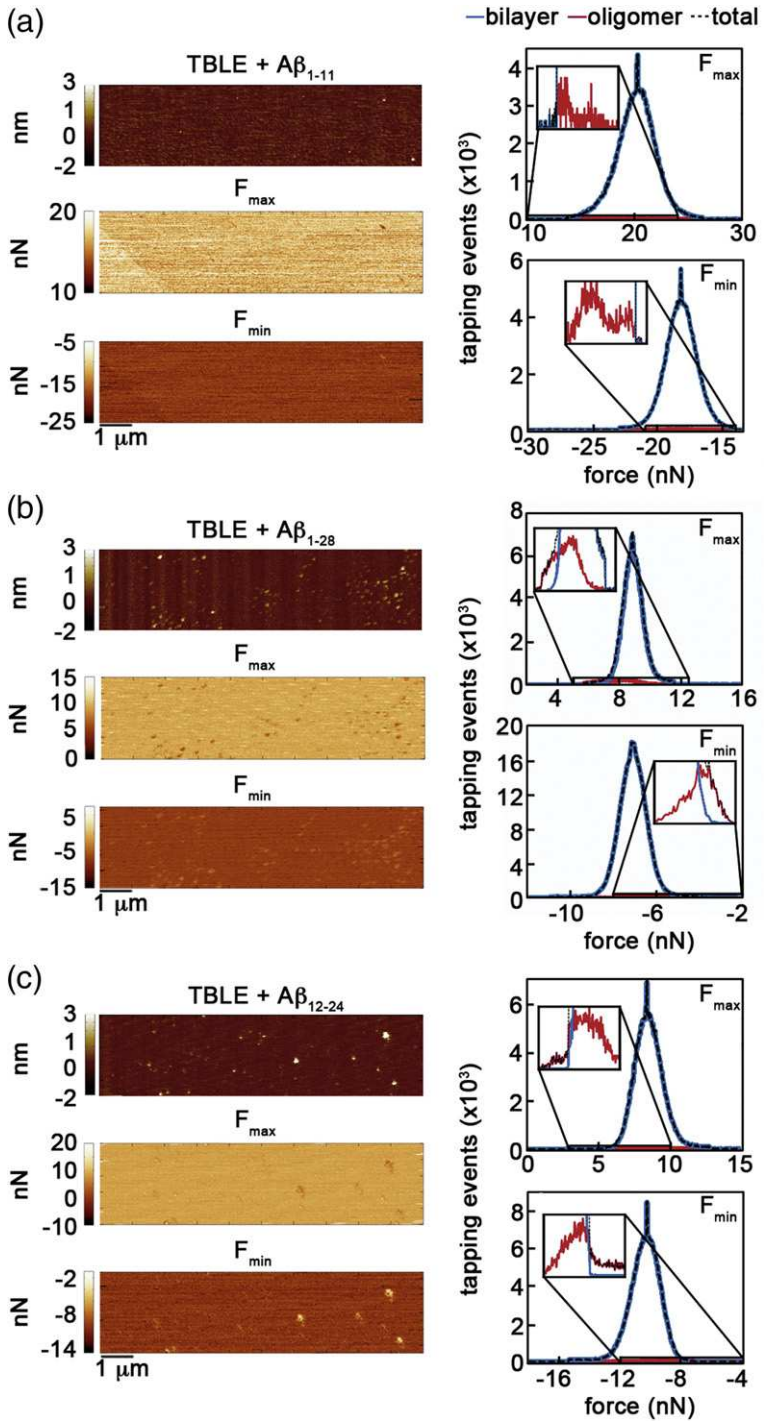

Fig. 6. Minimal changes in local mechanical properties of TBLE bilayers are associated with exposure to $A\beta_{1-11}$, $A\beta_{1-28}$, or $A\beta_{12-24}$. As $A\beta_{1-11}$, $A\beta_{1-28}$, and $A\beta_{12-24}$ only formed oligomeric aggregates on TBLE bilayer, extensive bilayer disruption was not observed. AFM topography, F_{max}, and F_{min} images of TBLE bilayer exposed to (a) $A\beta_{1-11}$, (b) $A\beta_{1-28}$, and (c) $A\beta_{12-24}$ were obtained using SPAM. Histograms of every tapping event (right of images) for F_{max} and F_{min} illustrate the various regions of interest: bilayer and oligomer, which were sorted based on the topography image. The insets zoom to show that the data associate with oligomers, as a significantly fewer tapping events are associated with these regions.

adhesive properties of a TBLE bilayer. To accomplish this, we used a technique called scanning probe acceleration microcopy (SPAM),[54] which recovers the time-resolved tip/sample force associated with every tapping event during the acquisition of a tapping mode AFM image taken in solution. Specific features of the tapping forces, the maximum tapping force (F_{max}) and minimum tapping force (F_{min}) per oscillation cycle, are sensitive to changes in the sample's mechanical properties and can be used to map these properties with high spatial resolution during regular AFM operation.[55,56] F_{max} is defined as the largest positive (or repulsive) force experienced between the tip and sample during one tapping event and is responsive to the sample's compression modulus. F_{min} is defined as the largest negative (or attractive) force between the tip and sample during one tapping event and is indicative of the adhesion

properties of the surface with respect to the probe. Topography, F_{max}, and F_{min} images of TBLE bilayers exposed to the different Aβ fragments for 16–20 h were generated (Figs. 6 and 7). Control topography, F_{max}, and F_{min} images are presented in Supplemental Fig. 2. These control images appear featureless, as the TBLE bilayer represents a relatively homogenous surface. As the topography and force data are obtained simultaneously, the tapping forces can be associated with specific topographical features, allowing for the deconvolution of the tapping force distributions. The fragments $Aβ_{1–11}$, $Aβ_{1–28}$, and $Aβ_{12–24}$, which only formed oligomeric aggregates on the TBLE bilayer, did not cause extensive mechanical changes in the bilayer (Fig. 6). However, the oligomers of these three fragments were typically less adherent to the probe and tended to be slightly more compressible.

The Aβ fragments that significantly altered the bilayer morphology and formed a larger variety of aggregates had a much larger impact on the mechanical properties (Fig. 7). For experiments performed with $Aβ_{10–26}$, $Aβ_{16–22}$, $Aβ_{22–35}$, or $Aβ_{1–40}$, portions of the bilayer were unaffected, and the forces associated with these areas can be used as an internal reference to determine the relative mechanical properties associated with different features of the surfaces. Whenever mica was exposed, those areas of the surface were associated with the highest magnitudes of F_{max} and F_{min}, consistent with mica being a hard substrate that is relatively more adherent to the probe. Based on F_{max}, the aggregates of $Aβ_{10–26}$, $Aβ_{16–22}$, $Aβ_{22–35}$, or $Aβ_{1–40}$ were more compressible compared with the bilayer, and F_{min} indicated that these aggregates were the features with the least amount of adhesion to the AFM tip. Regions of the bilayer that had disrupted bilayer morphology (for example in $Aβ_{1–40}$) were consistently more compressible (softer) than unperturbed regions of bilayer; however, these regions

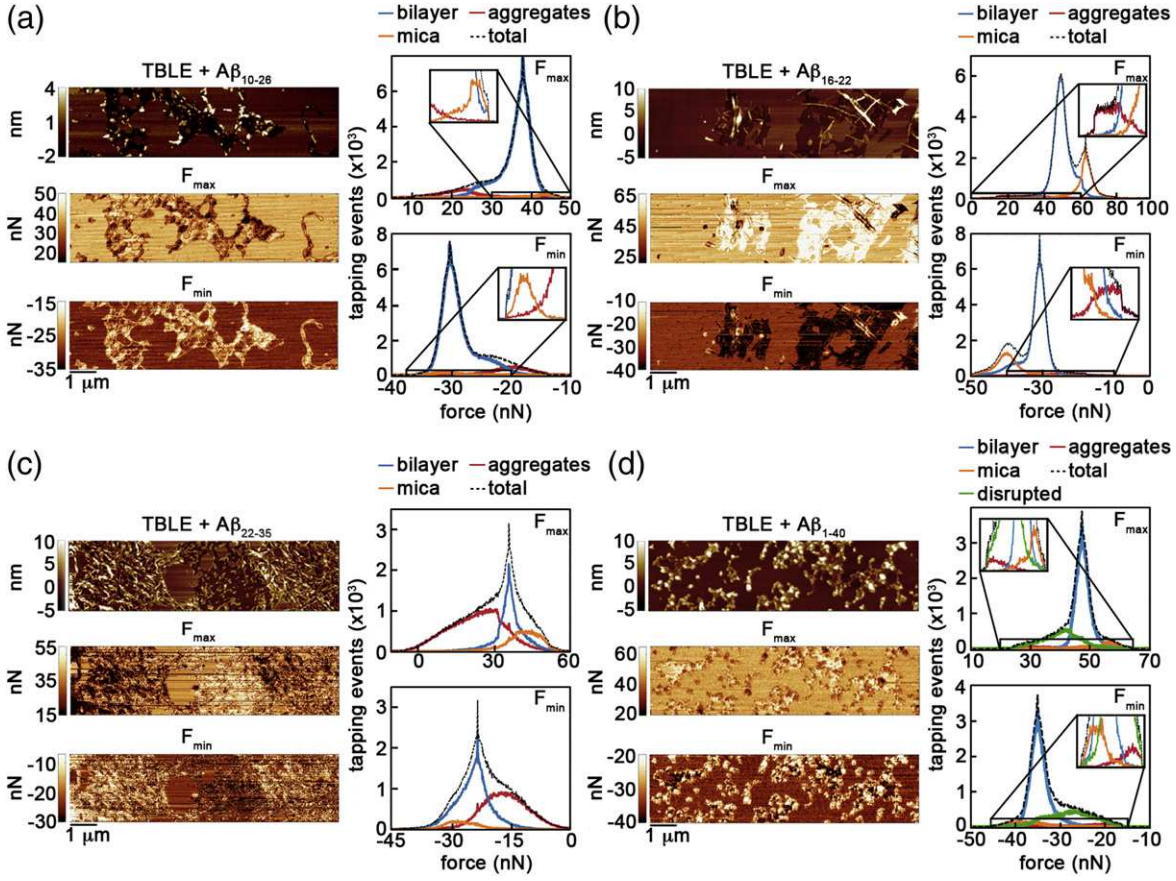

Fig. 7. $Aβ_{10–26}$, $Aβ_{16–22}$, $Aβ_{22–35}$, and $Aβ_{1–40}$ disrupt TBLE bilayers, altering the mechanical properties of the bilayer. AFM topography, F_{max}, and F_{min} images of TBLE bilayers exposed to (a) $Aβ_{10–26}$, (b) $Aβ_{16–22}$, (c) $Aβ_{22–35}$, and (d) $Aβ_{1–40}$ were obtained using SPAM. Histograms of every tapping event (right of images) for both F_{max} and F_{min} illustrate the various regions of interest: $Aβ_{10–26}$, $Aβ_{16–22}$, and $Aβ_{22–35}$; these regions include undisrupted bilayer, mica, and aggregates, whereas $Aβ_{1–40}$ showed regions of undisrupted bilayer and disrupted bilayer, mica, and aggregates. These regions were sorted based on the topography image. The insets zoom to show regions of the surface that have significantly fewer tapping events associated with them.

were not as soft as the actual aggregates. This is consistent with Aβ fragments reducing the ordering and packing efficiency of the bilayer,[57,58] resulting in a more compressible membrane.

Discussion

We have investigated a variety of Aβ fragments in an effort to understand how specific regions of Aβ regulate its interaction with lipid membranes. In particular, we investigated the interaction of $Aβ_{1–11}$, $Aβ_{1–28}$, $Aβ_{10–26}$, $Aβ_{12–24}$, $Aβ_{16–22}$, $Aβ_{22–35}$, and $Aβ_{1–40}$ with TBLE bilayers. These Aβ fragments represent a variety of chemically unique regions along the peptide, that is, the extracellular domain, β-strand, β-turns, the central hydrophobic core, and a portion of the transmembrane domain. While these studies using these Aβ fragments can provide insights into the interaction of specific domains with lipid membranes, care must be used in extrapolating these results in understanding the dynamic aggregation of full-length Aβ in solution or at lipid interfaces. Specifically, studies with these fragments exclude the potential of the interaction between protein domains to facilitate aggregation or binding to lipid membranes. Furthermore, the Aβ concentrations used in this study are large compared to those typically observed *in vivo*. While this was done to allow for observations within an experimentally feasible time period, this increased concentration must be taken into consideration when interpreting these results, as amyloid formation is highly dependent on protein concentration.

Exposure of the model lipid membrane to fresh preparations of these Aβ fragments resulted in distinct aggregation patterns and changes in bilayer stability associated with each fragment. $Aβ_{10–26}$, $Aβ_{16–22}$, $Aβ_{22–35}$, and $Aβ_{1–40}$ caused disruption of the lipid bilayer structure upon exposure and resulted in a variety of distinct fibrillar aggregates. Exposure to these fragments resulted in altered mechanical properties of the lipid bilayer. Interestingly, in the corresponding force images, we were able to determine the rigidity associated with individual aggregates of Aβ fragments bound to the membrane. The aggregates were more compressible than the surrounding lipid bilayer, indicating that the aggregate may form a local weak spot within the membrane that may lead to fragmentation of the membrane structure. Conversely, $Aβ_{1–11}$, $Aβ_{1–28}$, and $Aβ_{12–24}$ had minimal interaction with lipid membranes, forming only oligomers that were weakly adhered to the surface. These studies provide insight into the potential role of specific amino acid sequences within Aβ on aggregation and interactions with lipid membranes. As a result, we have determined that residues 16–23 and 30–35 play a major role in Aβ binding to model membranes and the subsequent changes in mechanical properties of the membrane. Similar sequences ($Aβ_{17–20}$ and $Aβ_{30–35}$) have been found to be critical in facilitating cellular toxicity and Aβ aggregation,[59] and portions of these regions (10 residues of the C-terminus and $Aβ_{17–21}$) have the greatest hydrophobic character of Aβ.[60]

While it would have been desirable to have a fragment representing just the transmembrane domain of Aβ, the preparatory protocol used in this study was unable to completely solubilize lyophilized stocks of such a fragment ($Aβ_{29–39}$). As it is well established that the chemical history of Aβ influences the aggregation pathway,[5,6] using a different preparation to solubilize $Aβ_{29–39}$ would have biased any comparisons with the other fragments. Presumably, the entire transmembrane domain would interact strongly with the hydrophobic core of a lipid membrane, as the $Aβ_{25–35}$ fragment, which only contains a portion of the transmembrane domain, interacted the most aggressively with TBLE in both the AFM and PDA assays. Observations from the literature further support this notion. Experiments with the same $Aβ_{25–35}$ fragment alters the structure and dynamic nature of a variety of phospholipid membranes.[61–63] An $Aβ_{25–40}$ fragment, which contains the entire transmembrane domain, preferentially localized within the hydrophobic core of DMPC/DPPG liposomes.[64] Interestingly, fragments of $Aβ_{31–35}$ and $Aβ_{25–35}$ can induce toxicity in PC12 cells, although by apparently different mechanisms as $Aβ_{31–35}$ toxicity is associated with biochemical features of apoptosis that are not detected in studies with $Aβ_{25–35}$.[65]

Surfaces have long been established as potential modifiers of amyloid formation, and our studies further demonstrate that lipid surfaces, in particular, can influence the aggregation of Aβ. It has been shown that chemically distinct surfaces influence the aggregation rate of Aβ, as well as the morphology.[14,15,66] Lateral mobility of Aβ appears to be critical in the formation of fibrils on solid surfaces and lipid bilayers,[67] and this could be important as single-molecule studies performed on Aβ inserted into anionic lipid membranes demonstrated high lateral mobility until aggregating into oligomers.[68] The affinity of Aβ for the surface also plays a role in creating local areas of high concentration that can lead to aggregation.[67] This factor is supported by our observations suggesting that Aβ fragments containing the transmembrane domain, with presumably a higher affinity for lipid membranes, aggregated more aggressively on TBLE bilayers.

The pathological action of Aβ and its aggregate forms appears to be at least partially attributable to interaction with cellular membranes.[69] Detrimental effects of Aβ on lipid membranes can occur via several potential mechanisms. Several studies have

indicated that Aβ can form pore-like structures in lipid membranes, resulting in increased membrane permeability.[31–34,70] Studies using lipid vesicles that contained self-quenching dyes have demonstrated that Aβ can disrupt the integrity of lipid bilayers, making them leaky,[71] and the disruption of bilayer morphology by Aβ has been observed by AFM for a variety of lipid systems.[21,25,32,72] The observed morphological changes in bilayers associated with Aβ fragments that aggressively interacted with the TBLE surface suggest that the aggregation process plays a role in altering the integrity of membranes.

The physical properties of lipid bilayers, such as phase state, bilayer curvature, elasticity and modulus, surface charge, and degree of hydration, can influence/modulate protein aggregation at membrane surfaces.[73] The lipid composition of a bilayer has been shown to exert substantial influence on the aggregation of amyloid-forming proteins.[26] We chose to use TBLE bilayers to study the aggregation of Aβ in the presence of a physiologically relevant mixture of lipid components. While this complicates the ability to determine the importance of specific Aβ/lipid interactions, other studies have indicated that the interaction of Aβ with membranes is highly dependent on the abundance of specific lipid components, that is, cholesterol,[24,74,75] sphingolipids,[76] gangliosides,[77] and neutral or charged phospholipids.[78–80] Neutral PC lipids extend the lag time needed to initiate Aβ aggregation in a concentration-dependent manner.[80] A variety of lipids have been shown to induce structural transition in Aβ, from α-helical to β-sheet, using circular dichroism.[78] The charge of the lipid membrane, which is determined by phospholipid headgroups, is a major factor controlling the extent of Aβ/membrane association, as the affinity of monomeric Aβ is stronger for membranes composed of negatively charged 1-palmitoyl-2-oleoyl-sn-glycero-3-phosphoglycerol compared with membranes of neutral 1-palmitoyl-2-oleoyl-sn-glycero-3-phosphocholine.[81,82] However, aggregation can modulate these interactions as fibrillization reduces the affinity for negatively charged membranes to a greater extent than that for neutral membranes.[82] Other studies demonstrate that Aβ binding to gangliosides accelerates fibril formation in the presence of vesicles.[83,84] Incorporation of gangliosides in membranes also facilitates the formation of Aβ pores and membrane fragmentation.[85] Ganglioside GM1 and sphingomyelin can destabilize mature Aβ fibrils, stabilizing intermediate protofibrillar aggregates.[86] Furthermore, altering the composition of supported TBLE bilayers by exposing them to apoE-containing lipoprotein particles was shown to reduce Aβ binding to the lipid surface, resulting in decreased membrane disruption.[21]

While previous studies using $A\beta_{1-40}$ mutants demonstrated that lipid membrane association of Aβ is driven by electrostatic and hydrophobic interactions,[22] our results indicate that specific domains also play an important role, leading to various degrees of lipid interaction and disruption. Understanding the interaction of specific Aβ residues with lipid membranes is important because Aβ may exert its cytotoxic effect at cellular membranes, not in free solution, changing the effectiveness of potential therapeutics that target Aβ. This concept has been demonstrated by studies on the aggregation of human islet amyloid polypeptide at phospholipid surfaces that showed that a known inhibitor of amyloid formation, (–)-epigallocatechin gallate, was less effective at a phospholipid interface.[87]

While the physical/chemical properties of bilayers may dictate the susceptibility of a membrane to Aβ binding, once Aβ binds the membrane, it can destabilize membrane structure, compromising membrane integrity. Aβ fragments that aggressively aggregated on TBLE bilayers created regions of disrupted bilayer morphology that were associated with a softer elastic modulus and reduced adhesion to the AFM probe tip in comparison to the unperturbed bilayer. A potential explanation for these observed changes in bilayers exposed to specific Aβ fragments is a decrease in the efficiency of the packing of the lipid components within the bilayer in response to protein insertion/binding and aggregation. This would lead to a rougher bilayer that is more easily compressed and a decrease in the number of potential hydrogen bonds formed between the tip and bilayer surface, leading to the lower adhesive interaction. This scenario is consistent with NMR studies that indicate that Aβ induces greater packing disorder in model lipid bilayers[57,58,85] and morphological changes associated with membrane exposure to Aβ observed here and elsewhere by AFM.[21–23] Furthermore, exposure to Aβ has been demonstrated to reduce the force necessary to puncture lipid membranes.[72] Rearrangement of lipid orientation should have profound effects on the mechanical integrity of membranes. While anisotropy studies with single-component lipid membranes demonstrated that monomeric Aβ had minimal impact on bilayer fluidity, oligomers decreased the lateral mobility of lipid components.[88] Evidence also suggests that polymorphic oligomeric structures have varying abilities to alter membrane fluidity,[88] and a reduction in membrane fluidity due to Aβ has been demonstrated in rodent brains.[89] Even at nanomolar concentrations, the lysis tension of unilamellar vesicles containing oxysterols can be altered by exposure to Aβ.[90] Here, we demonstrate that specific Aβ fragments can locally increase the compressibility of TBLE bilayers and in some cases even generate holes spanning the entire membrane. Collectively, these results suggest that Aβ can negatively impact the mechanical integrity of lipid membranes.

Aβ can also induce membrane curvature in DOPC lipid vesicles, inducing several different vesicle

shapes.[91] These changes in vesicle curvature were highly dependent on the aggregation state of Aβ, and the mechanical strain associated with Aβ-induced curvature of lipid membranes could lead directly to their disruption. Such a mechanism has also been demonstrated for the interaction of the islet amyloid polypeptide with lipid vesicles.[92–94] However, due to our AFM studies being performed on bilayers supported by a solid substrate, we were unable to determine if the fragments studied here preferentially induced large-scale changes in membrane curvature.

$A\beta_{1–11}$, $A\beta_{1–28}$, and $A\beta_{12–24}$ did not extensively aggregate on TBLE bilayers (only oligomers were observed) and did not result in detectable membrane disruption. This is easily explained for $A\beta_{1–11}$, which represents the N-terminus of the hydrophilic extracellular domain and contains no β-sheet-forming sequences. However, both $A\beta_{1–28}$ and $A\beta_{12–24}$ contain extensive hydrophobic residues that have been associated with β-strand formation. Presumably, these should have interacted with the lipid bilayer. However, the addition of the first 11 residues of Aβ in $A\beta_{1–28}$ may impede the lipid/protein interaction. This notion is supported by circular dichroism studies demonstrating that the random structure of $A\beta_{1–28}$ is unchanged in the presence of a TBLE bilayer.[25] It is not entirely clear, however, why $A\beta_{12–24}$ did not interact extensively with the bilayer when $A\beta_{10–26}$ and $A\beta_{16–22}$ did.

Based on our morphological and mechanical observations, we propose three scenarios for the impact of Aβ and its aggregate forms on bilayer structure (Fig. 8). Due to the lack of structural information at the molecular level, these scenarios are somewhat speculative. Monomers or small oligomers (i.e., dimers) can penetrate into the bilayer structure, resulting in disordering of the bilayer structure that manifest as increased surface roughness observed in AFM images (Fig. 8a). This insertion into the bilayer by the Aβ fragments is facilitated by the presence of the central hydrophobic core and/or the transmembrane domain. Depending on the specific fragment studied, oligomers are located within regions of increased bilayer roughness, or not associated with changes in bilayer morphology (Fig. 8b). Presumably, the oligomers that perturbed the bilayer morphology were partially inserted into the membrane, forcing the rearrangement of lipid components to accommodate the presence of the oligomer. Oligomers that minimally inserted into the bilayer would not cause observable bilayer roughening. The bilayer roughening associated with monomers and oligomers can potentially lead to membrane leakage and dysfunction. The formation of fibrils of the Aβ fragments on the bilayer was often associated with fragmentation of the membrane, exposing bare mica substrate (Fig. 8c). Collectively, the ability of Aβ and its aggregate forms to bind lipid membranes and impact their structural integrity can potentially play a role in a variety of toxic mechanisms associated with AD.

Materials and Methods

Peptide preparation

Synthetic fragments of $A\beta_{1–11}$, $A\beta_{1–28}$, $A\beta_{10–26}$, $A\beta_{12–24}$, $A\beta_{16–22}$, $A\beta_{22–35}$, and $A\beta_{1–40}$ (AnaSpec Inc., San Jose, CA) were prepared in the same manner according to published protocols.[46] Briefly, peptides were treated with hexafluoroisopropanol to dissolve seeds and preexisting aggregates within the lyophilized stock. Hexafluoroisopropanol was evaporated off in a Vacufuge concentrator (Eppendorf), resulting in peptide films. These peptide films were dissolved in 10 μL of dimethyl sulfoxide to make a 2000-μM stock solution. To achieve a final concentration of 20 μM, we dissolved the stock solutions directly into 37 °C phosphate-buffered saline (PBS) buffer (pH 7.3). The molecular masses of these fragments are 1.33 kDa for $A\beta_{1–11}$, 3.26 kDa for $A\beta_{1–28}$, 2.01 kDa for $A\beta_{10–26}$, 1.57 kDa for $A\beta_{12–24}$, 0.85 kDa for $A\beta_{16–22}$, 1.40 kDa for $A\beta_{22–35}$, and 4.33 kDa for $A\beta_{1–40}$.

Preparation of defect-free bilayers

Lyophilized porcine TBLE (Avanti Polar Lipids, Alabaster, AL) was resuspended in PBS (pH 7.3) at a concentration of 1 mg/mL. Using an acetone/dry ice bath, we formed bilayers and multilayer lipid sheets by five cycles of

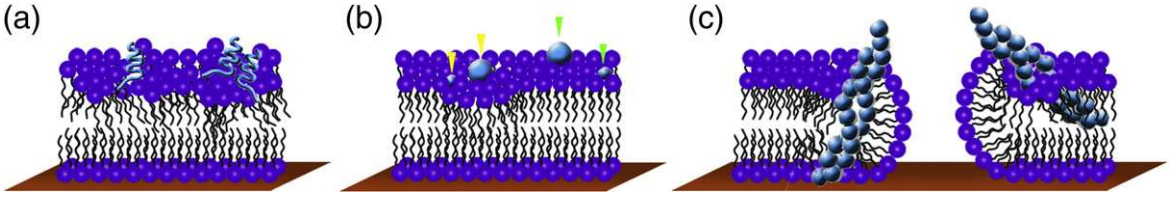

Fig. 8. Aβ fragments can interact with lipid bilayers via several potential scenarios. (a) Monomeric or small oligomeric species (i.e., dimers) can insert into bilayers, creating disorder within the membrane. (b) Oligomers of Aβ fragments can be loosely adhered to the surface of the bilayer (green arrows) or partially inserted into the bilayer (yellow arrows). When oligomers insert into the bilayer, they displace lipid components. (c) Fibril formation at the membrane surface leads to lipid disordering and eventual fragmentation of the membrane, exposing the underlying mica substrate.

freeze–thaw treatment.[25] Lipid suspensions were then sonicated for 15 min to promote vesicle formation. Next, 15 μL of a 1:1 TBLE/PBS (pH 7.3) solution was injected directly into a prepared AFM fluid cell. A defect-free bilayer (40 × 40 μm) was formed via vesicle fusion on a freshly cleaved mica substrate. Once formed, two to three washes with PBS were performed to remove excess lipid vesicles from the fluid cell. All experiments were performed with the same lot of lipids.

PDA assay

PDA assay was prepared using previously reported protocols.[53,95] In short, the diacetylene monomers 10,12-tricosadiynoic acid (GFS Chemicals, Columbus, OH) and TBLE (2:3 molar ratio) were dissolved in a solution of 1:1 chloroform/ethanol. The solution was rotovapped off, leaving a thin, dry film. 1× Tris-buffered saline (TBS) heated to 70 °C was added to the film and sonicated for 5 min at 100 W using a sonic dismembrator (FisherSci). To ensure self-assembly of the vesicles, we stored the suspension at 4 °C overnight. The suspension was polymerized by irradiation at 254 nm with 7 lumens for 10 min (room temperature with stirring) turning a brilliant blue. The assay included polymerized PDA + 1× TBS (negative control), polymerized PDA + 1× TBS + NaOH (pH 12) (positive control), and polymerized PDA + 1× TBS + Aβ for each individual Aβ sequence with a final protein concentration of 20 μM. CR over 24 h for each well was recorded using an Infinite M1000 Pro plate reader (TECAN, Switzerland) at 37 °C measuring both the blue component (640 nm) and the red component (500 nm) of the spectrum.

AFM imaging conditions

For *ex situ* AFM imaging, 20-μM solutions of each sequence were prepared and incubated at 37 °C with no shaking for the duration of the experiment. Aliquots (2 μL) of each incubation were spotted onto freshly cleaved mica for 30 s at various time points, washed with 200 μL of high-pressure liquid chromatography-grade water, and dried under a gentle stream of nitrogen. Deposited peptide aggregates were imaged with a Nanoscope V MultiMode scanning probe microscope (Veeco, Santa Barbara, CA) equipped with a closed-loop vertical engage J-scanner and operated in tapping mode. *Ex situ* images were acquired with diving-board-shaped silicon cantilevers with a nominal spring constant of 40 N/m and resonance frequency of ~300 kHz.

For *in situ* AFM experiments, the Nanoscope V MultiMode scanning probe microscope (Veeco) was operated in tapping mode, equipped with a fluid cell sealed with an O-ring. *In situ* images were obtained with V-shaped oxide-sharpened silicon nitride cantilevers with a nominal spring constant of 0.5 N/m (Budget Sensors, Bulgaria). Scan rates were set at 1–2 Hz with cantilever drive frequencies ranging from ~8 to 10 kHz. Thirty-five microliters of filtered PBS buffer was added to the fluid cell, and background images were obtained to ensure cleanliness of the cell before direct injection of 15 μL of TBLE solution. Once formed, only defect-free TBLE bilayers that were 40 × 40 μm were exposed to Aβ fragments at a final concentration of 20 μM. Upon injection of the sequence, a 10 × 10 μm image of the surface with 1024 × 1024 pixel resolution was taken before sealing the fluid cell to prevent evaporation. The bilayer was imaged again 16–20 h after exposure to the Aβ fragments.

For SPAM experiments, 10 × 2.5 μm images were captured with 512 × 128 pixel resolution. Cantilever deflection trajectories were captured at 2.5 MS/s and 14-bit resolution with a vertical range of 2 V via a combination of a signal access module (Veeco) and CompuScope 14100 data acquisition card (Gage, Lachine, Quebec). A Fourier-transform-based harmonic comb filter was applied to the deflection signal, and the second derivative of the filtered cantilever deflection was used to obtain the time-resolved tip acceleration. By use of the effective mass, m_{eff}, of the cantilever, the time-resolved tapping force between the tip and sample was recovered.[54] m_{eff} was determined using a thermal tuning method by obtaining the spring constant and resonance frequency of the cantilever.

Quantitative image analysis

AFM image analysis was performed using the image processing toolbox of Matlab (MathWorks, Natick, MA) as described elsewhere.[96] Briefly, the physical dimensions of aggregates were measured automatically by (1) importing images into Matlab, (2) flattening the images to correct for background curvature, (3) using a height threshold to create a binary map of the surface that can be used to locate individual aggregates, and (4) implementing pattern recognition algorithms to the binary map to locate aggregates and measure specific features (height, volume, contour length, etc.) of each individual aggregate. To determine fibril contour length and end-to-end distance, we used a fast parallel thinning algorithm[97] to create a pixel skeleton of each object present in the AFM image. Once the pixel skeletons of fibrils were obtained, crossing over points of slightly entangled fibrils were removed, and the endpoints of each skeleton was determined.[98] Highly entangled skeletons were removed from the analysis. The end-to-end length between the endpoints connected by a pixel skeleton was calculated, and the contour length was calculated based on the length of the entire pixel skeleton.

Acknowledgements

The authors acknowledge Dr. Jonathan Boyd and Julie Vrana for access and assistance in using the TECAN plate reader. This work was funded by the Brodie Discovery and Innovation fund, the National Science Foundation (NSF#1054211), and the Alzheimer's Association (NIRG-11-203834). E.M.C. was supported by the Center for Neuroscience Summer Undergraduate Research Internship program (Robert C. Byrd Health Sciences Center, West Virginia University). M.F.L. was supported by the Honors Summer Undergraduate Research Experience program (The Honors College at West Virginia University). C.S.U. was supported by NanoSURE (WVNano, West Virginia University).

Author Contributions. E.A.Y and J.L. conceived the experiments. E.A.Y accomplished all peptide preparation, performed and analyzed all lipid experiments, and analyzed all *ex situ* experiments. S.L.O. and C.S.U. developed, performed, and analyzed the PDA experiments. M.F.L. and E.M.C performed *ex situ* experiments. E.M.C. and S.L.O. assisted with peptide preparation. E.A.Y and J.L. wrote and edited the paper.

Supplementary Data

Supplementary data to this article can be found online at http://dx.doi.org/10.1016/j.jmb.2013.03.022

Received 15 November 2012;
Received in revised form 9 February 2013;
Accepted 4 March 2013
Available online 21 March 2013

Keywords:
amyloid;
Alzheimer's disease;
atomic force microscopy;
protein aggregation;
scanning probe acceleration microscopy

Abbreviations used:
Aβ, β-amyloid peptide; AD, Alzheimer's disease; AFM, atomic force microscopy; CR, colorimetric response; PBS, phosphate-buffered saline; PDA, polydiacetylene; SPAM, scanning probe acceleration microcopy; TBLE, total brain lipid extract; TBS, Tris-buffered saline.

References

1. McGeer, P. L. & McGeer, E. G. (1995). The inflammatory response system of brain: Implications for therapy of Alzheimer and other neurodegenerative diseases. *Brain Res. Rev.* **21**, 195–218.
2. Haass, C. & Selkoe, D. J. (2007). Soluble protein oligomers in neurodegeneration: lessons from the Alzheimer's amyloid beta-peptide. *Nat. Rev. Mol. Cell Biol.* **8**, 101–112.
3. DeToma, A. S., Salamekh, S., Ramamoorthy, A. & Lim, M. H. (2012). Misfolded proteins in Alzheimer's disease and type II diabetes. *Chem. Soc. Rev.* **41**, 608–621.
4. Goldsbury, C., Wirtz, S., Muller, S., Sunderji, S., Wicki, P., Aebi, U. & Frey, P. (2000). Studies on the in vitro assembly of Aβ 1–40: implications for the search for a beta fibril formation inhibitors. *J. Struct. Biol.* **130**, 217–231.
5. Kodali, R. & Wetzel, R. (2007). Polymorphism in the intermediates and products of amyloid assembly. *Curr. Opin. Struct. Biol.* **17**, 48–57.
6. Kodali, R., Williams, A. D., Chemuru, S. & Wetzel, R. (2010). Aβ(1–40) forms five distinct amyloid structures whose beta-sheet contents and fibril stabilities are correlated. *J. Mol. Biol.* **401**, 503–517.
7. Meinhardt, J., Sachse, C., Hortschansky, P., Grigorieff, N. & Fandrich, M. (2009). Aβ(1–40) fibril polymorphism implies diverse interaction patterns in amyloid fibrils. *J. Mol. Biol.* **386**, 869–877.
8. Barnham, K. J., Masters, C. L. & Bush, A. I. (2004). Neurodegenerative diseases and oxidative stress. *Nat. Rev. Drug Discov.* **3**, 205–214.
9. Bolognin, S., Drago, D., Messori, L. & Zatta, P. (2009). Chelation therapy for neurodegenerative diseases. *Med. Res. Rev.* **29**, 547–570.
10. Bonda, D. J., Lee, H.-g, Blair, J. A., Zhu, X., Perry, G. & Smith, M. A. (2011). Role of metal dyshomeostasis in Alzheimer's disease. *Metallomics*, **3**, 267–270.
11. Braymer, J. J., Choi, J.-S., DeToma, A. S., Wang, C., Nam, K., Kampf, J. W. *et al.* (2011). Development of bifunctional stilbene derivatives for targeting and modulating metal-amyloid-beta species. *Inorg. Chem.* **50**, 10724–10734.
12. Hindo, S. S., Mancino, A. M., Braymer, J. J., Liu, Y., Vivekanandan, S., Ramamoorthy, A. & Lim, M. H. (2009). Small molecule modulators of copper-induced Aβ aggregation. *J. Am. Chem. Soc.* **131**, 16663–16665.
13. Jones, M. R., Service, E. L., Thompson, J. R., Wang, M. C. P., Kimsey, I. J., DeToma, A. S. *et al.* (2012). Dual-function triazole–pyridine derivatives as inhibitors of metal-induced amyloid-beta aggregation. *Metallomics*, **4**, 910–920.
14. Kowalewski, T. & Holtzman, D. M. (1999). In situ atomic force microscopy study of Alzheimer's β-amyloid peptide on different substrates: new insights into mechanism of beta-sheet formation. *Proc. Natl Acad. Sci. USA*, **96**, 3688–3693.
15. Moores, B., Drolle, E., Attwood, S. J., Simons, J. & Leonenko, Z. (2011). Effect of surfaces on amyloid fibril formation. *PLoS One*, **6**, e25954.
16. Morriss-Andrews, A. & Shea, J. E. (2012). Kinetic pathways to peptide aggregation on surfaces: the effects of beta-sheet propensity and surface attraction. *J. Chem. Phys.* **136**, 065103.
17. Yates, E. A., Cucco, E. M. & Legleiter, J. (2011). Point mutations in Aβ induce polymorphic aggregates at liquid/solid interfaces. *ACS Chem. Neurosci.* **2**, 294–307.
18. Linse, S., Cabaleiro-Lago, C., Xue, W.-F., Lynch, I., Lindman, S., Thulin, E. *et al.* (2007). Nucleation of protein fibrillation by nanoparticles. *Proc. Natl Acad. Sci. USA*, **104**, 8691–8696.
19. Yoo, S. I., Yang, M., Brender, J. R., Subramanian, V., Sun, K., Joo, N. E. *et al.* (2011). Inhibition of amyloid peptide fibrillation by inorganic nanoparticles: functional similarities with proteins. *Angew. Chem. Int. Edit.* **50**, 5110–5115.
20. Petkova, A. T., Leapman, R. D., Guo, Z. H., Yau, W. M., Mattson, M. P. & Tycko, R. (2005). Self-propagating, molecular-level polymorphism in Alzheimer's beta-amyloid fibrils. *Science*, **307**, 262–265.
21. Legleiter, J., Fryer, J. D., Holtzman, D. M. & Kowalewski, A. (2011). The modulating effect of mechanical changes in lipid bilayers caused by apoE-containing lipoproteins on Aβ induced membrane disruption. *ACS Chem. Neurosci.* **2**, 588–599.
22. Pifer, P. M., Yates, E. A. & Legleiter, J. (2011). Point mutations in Aβ result in the formation of distinct

polymorphic aggregates in the presence of lipid bilayers. *PLoS One*, **6**, e16248.
23. Yip, C. M., Darabie, A. A. & McLaurin, J. (2002). Aβ 42-peptide assembly on lipid bilayers. *J. Mol. Biol.* **318**, 97–107.
24. Yip, C. M., Elton, E. A., Darabie, A. A., Morrison, M. R. & McLaurin, J. (2001). Cholesterol, a modulator of membrane-associated Aβ-fibrillogenesis and neurotoxicity. *J. Mol. Biol.* **311**, 723–734.
25. Yip, C. M. & McLaurin, J. (2001). Amyloid-β peptide assembly: a critical step in fibrillogenesis and membrane disruption. *Biophys. J.* **80**, 1359–1371.
26. Evangelisti, E., Cecchi, C., Cascella, R., Sgromo, C., Becatti, M., Dobson, C. M. *et al.* (2012). Membrane lipid composition and its physicochemical properties define cell vulnerability to aberrant protein oligomers. *J. Cell Sci.* **125**, 2416–2427.
27. Simakova, O. & Arispe, N. J. (2007). The cell-selective neurotoxicity of the Alzheimer's Aβ peptide is determined by surface phosphatidylserine and cytosolic ATP levels membrane binding is required for Aβ toxicity. *J. Neurosci.* **27**, 13719–13729.
28. Simakova, O. & Arispe, N. J. (2011). Fluorescent analysis of the cell-selective Alzheimer's disease Aβ peptide surface membrane binding: influence of membrane components. *Int. J. Alzheimers Dis.* **2011**, 917629.
29. Friedman, R., Pellarin, R. & Caflisch, A. (2009). Amyloid aggregation on lipid bilayers and its impact on membrane permeability. *J. Mol. Biol.* **387**, 407–415.
30. Michikawa, M., Gong, J. S., Fan, Q. W., Sawamura, N. & Yanagisawa, K. (2001). A novel action of Alzheimer's amyloid β-protein (Aβ): oligomeric Aβ promotes lipid release. *J. Neurosci.* **21**, 7226–7235.
31. Capone, R., Jang, H., Kotler, S. A., Kagan, B. L., Nussinov, R. & Lal, R. (2012). Probing structural features of Alzheimer's amyloid-beta pores in bilayers using site-specific amino acid substitutions. *Biochemistry*, **51**, 776–785.
32. Connelly, L., Jang, H., Arce, F. T., Capone, R., Kotler, S. A., Ramachandran, S. *et al.* (2012). Atomic force microscopy and MD simulations reveal pore-like structures of all-D-enantiomer of Alzheimer's β-amyloid peptide: relevance to the ion channel mechanism of AD pathology. *J. Phys. Chem. B*, **116**, 1728–1735.
33. Jang, H., Zheng, J. & Nussinov, R. (2007). Models of beta-amyloid ion channels in the membrane suggest that channel formation in the bilayer is a dynamic process. *Biophys. J.* **93**, 1938–1949.
34. Lashuel, H. A., Hartley, D. M., Petre, B. M., Wall, J. S., Simon, M. N., Walz, T. & Lansbury, P. T. (2003). Mixtures of wild-type and a pathogenic (E22G) form of A beta 40 in vitro accumulate protofibrils, including amyloid pores. *J. Mol. Biol.* **332**, 795–808.
35. Barrow, C. J., Yasuda, A., Kenny, P. T. M. & Zagorski, M. G. (1992). Solution conformations and aggregational properties of synthetic amyloid beta-peptides of Alzheimers disease - analayis of circular-dichrosism spectra. *J. Mol. Biol.* **225**, 1075–1093.
36. Barrow, C. J. & Zagorski, M. G. (1991). Solution structures of beta peptide and its constituent fragments—relation to amyloid deposition. *Science*, **253**, 179–182.
37. Inouye, H., Fraser, P. E. & Kirschner, D. A. (1993). Structure of beta-crystallite assemblies formed by Alzheimer beta-amyloid protein analogs—analysis by X-ray diffraction. *Biophys. J.* **64**, 502–519.
38. Torok, M., Milton, S., Kayed, R., Wu, P., McIntire, T., Glabe, C. G. & Langen, R. (2002). Structural and dynamic features of Alzheimer's Aβ peptide in amyloid fibrils studied by site-directed spin labeling. *J. Biol. Chem.* **277**, 40810–40815.
39. Antzutkin, O. N., Balbach, J. J., Leapman, R. D., Rizzo, N. W., Reed, J. & Tycko, R. (2000). Multiple quantum solid-state NMR indicates a parallel, not antiparallel, organization of β-sheets in Alzheimer's β-amyloid fibrils. *Proc. Natl Acad. Sci. USA*, **97**, 13045–13050.
40. Tycko, R. (2006). Solid-state NMR as a probe of amyloid structure. *Protein Pept. Lett.* **13**, 229–234.
41. Buchete, N. V., Tycko, R. & Hummer, G. (2005). Molecular dynamics simulations of Alzheimer's β-amyloid protofilaments. *J. Mol. Biol.* **353**, 804–821.
42. Pastor, M. T., Kuemmerer, N., Schubert, V., Esteras-Chopo, A., Dotti, C. G., de la Paz, M. L. & Serrano, L. (2008). Amyloid toxicity is independent of polypeptide sequence, length and chirality. *J. Mol. Biol.* **375**, 695–707.
43. Lazo, N. D., Grant, M. A., Condron, M. C., Rigby, A. C. & Teplow, D. B. (2005). On the nucleation of amyloid β-protein monomer folding. *Protein Sci.* **14**, 1581–1596.
44. Hou, L. M., Shao, H. Y., Zhang, Y. B., Li, H., Menon, N. K., Neuhaus, E. B. *et al.* (2004). Solution NMR studies of the Aβ(1–40) and Aβ(1–42) peptides establish that the met35 oxidation state affects the mechanism of amyloid formation. *J. Am. Chem. Soc.* **126**, 1992–2005.
45. Vivekanandan, S., Brender, J. R., Lee, S. Y. & Ramamoorthy, A. (2011). A partially folded structure of amyloid-β(1–40) in an aqueous environment. *Biochem. Biophys. Res. Commun.* **411**, 312–316.
46. Stine, W. B., Dahlgren, K. N., Krafft, G. A. & LaDu, M. J. (2003). In vitro characterization of conditions for amyloid-β peptide oligomerization and fibrillogenesis. *J. Biol. Chem.* **278**, 11612–11622.
47. Legleiter, J., DeMattos, R. B., Holtzman, D. M. & Kowalewski, T. (2004). In situ AFM studies of astrocyte-secreted apolipoprotein E- and J-containing lipoproteins. *J. Colloid Interf. Sci.* **278**, 96–106.
48. Anfinsen, C. B. (1973). Principles that govern the folding of protein chains. *Science*, **181**, 223–230.
49. Derjaguin, B. V., Muller, V. M. & Toporov, Y. P. (1975). Effect of contact deformations on the adhesion of particles. *J. Colloid Interf. Sci.* **53**, 314–326.
50. Groves, J. T., Ulman, N. & Boxer, S. G. (1997). Micropatterning fluid lipid bilayers on solid supports. *Science*, **275**, 651–653.
51. Jass, J., Tjarnhage, T. & Puu, G. (2000). From liposomes to supported, planar bilayer structures on hydrophilic and hydrophobic surfaces: an atomic force microscopy study. *Biophys. J.* **79**, 3153–3163.
52. Jelinek, R. & Kolusheva, S. (2007). In *Biomolecular Sensing with Colorimetric Vesicles Creative Chemical Sensor Systems* (Schrader, T., ed.), 277, pp. 155–180. Springer, Berlin/Heidelberg.
53. Sokolovski, M., Sheynis, T., Kolusheva, S. & Jelinek, R. (2008). Membrane interactions and lipid binding of

casein oligomers and early aggregates. *Biochim. Biophys. Acta*, **1778**, 2341–2349.
54. Legleiter, J., Park, M., Cusick, B. & Kowalewski, T. (2006). Scanning probe acceleration microscopy (SPAM) in fluids: mapping mechanical properties of surfaces at the nanoscale. *Proc. Natl Acad. Sci. USA*, **103**, 4813–4818.
55. Shamitko-Klingensmith, N., Molchanoff, K. M., Burke, K. A., Magnone, G. J. & Legleiter, J. (2012). Mapping the mechanical properties of cholesterol-containing supported lipid bilayers with nanoscale spatial resolution. *Langmuir*, **28**, 13411–13422.
56. Burke, K. A., Yates, E. A. & Legleiter, J. (2013). Amyloid-forming proteins alter the local mechanical properties of lipid membranes. *Biochemistry*, **52**, 808–817.
57. Bokvist, M., Lindstrom, F., Watts, A. & Grobner, G. (2004). Two types of Alzheimer's β-amyloid (1–40) peptide membrane interactions: aggregation preventing transmembrane anchoring versus accelerated surface fibril formation. *J. Mol. Biol.* **335**, 1039–1049.
58. Lindstrom, F., Bokvist, M., Sparrman, T. & Grobner, G. (2002). Association of amyloid-β peptide with membrane surfaces monitored by solid state NMR. *Phys. Chem. Chem. Phys.* **4**, 5524–5530.
59. Liu, R., McAllister, C., Lyubchenko, Y. & Sierks, M. R. (2004). Residues 17–20 and 30–35 of β-amyloid play critical roles in aggregation. *J. Neurosci. Res.* **75**, 162–171.
60. Soto, C., Branes, M. C., Alvarez, J. & Inestrosa, N. C. (1994). Structural determinants of the Alzheimer's amyloid β-peptide. *J. Neurochem.* **63**, 1191–1198.
61. Buchsteiner, A., Hauss, T., Dante, S. & Dencher, N. A. (2010). Alzheimer's disease amyloid-β peptide analogue alters the ps-dynamics of phospholipid membranes. *Biochim. Biophys. Acta*, **1798**, 1969–1976.
62. Dante, S., Hauss, T. & Dencher, N. A. (2002). β-amyloid 25 to 35 is intercalated in anionic and zwitterionic lipid membranes to different extents. *Biophys. J.* **83**, 2610–2616.
63. Dante, S., Hauss, T. & Dencher, N. A. (2003). Insertion of externally administered amyloid beta peptide 25–35 and perturbation of lipid bilayers. *Biochemistry*, **42**, 13667–13672.
64. Ionov, M., Klajnert, B., Gardikis, K., Hatziantoniou, S., Palecz, B., Salakhutdinov, B. *et al.* (2010). Effect of amyloid-β peptides Aβ(1–28) and Aβ(25–40) on model lipid membranes. *J. Therm. Anal. Calorim.* **99**, 741–747.
65. Misiti, F., Sampaolese, B., Pezzotti, M., Marini, S., Coletta, M., Ceccarelli, L. *et al.* (2005). Aβ(31–35) peptide induce apoptosis in PC 12 cells: contrast with Aβ(25–35) peptide and examination of underlying mechanisms. *Neurochem. Int.* **46**, 575–583.
66. Blackley, H. K. L., Sanders, G. H. W., Davies, M. C., Roberts, C. J., Tendler, S. J. B. & Wilkinson, M. J. (2000). In-situ atomic force microscopy study of β-amyloid fibrillization. *J. Mol. Biol.* **298**, 833–840.
67. Shen, L., Adachi, T., Bout, D. V. & Zhu, X. Y. (2012). A mobile precursor determines amyloid-β peptide fibril formation at interfaces. *J. Am. Chem. Soc.* **134**, 14172–14178.
68. Ding, H., Schauerte, Joseph A., Steel, Duncan G. & Gafni, A. (2012). β-Amyloid (1–40) peptide interactions with supported phospholipid membranes: a single-molecule study. *Biophys. J.* **103**, 1500–1509.
69. Williams, T. L. & Serpell, L. C. (2011). Membrane and surface interactions of Alzheimer's Aβ peptide—insights into the mechanism of cytotoxicity. *FEBS J.* **278**, 3905–3917.
70. Connelly, L., Jang, H., Arce, F. T., Ramachandran, S., Kagan, B. L., Nussinov, R. & Lal, R. (2012). Effects of point substitutions on the structure of toxic Alzheimer's β-amyloid channels: atomic force microscopy and molecular dynamics simulations. *Biochemistry*, **51**, 3031–3038.
71. Williams, T. L., Day, I. J. & Serpell, L. C. (2010). The effect of Alzheimer's Aβ aggregation state on the permeation of biomimetic lipid vesicles. *Langmuir*, **26**, 17260–17268.
72. Dante, S., Hauss, T., Steitz, R., Canale, C. & Dencher, N. A. (2011). Nanoscale structural and mechanical effects of β-amyloid (1–42) on polymer cushioned membranes: a combined study by neutron reflectometry and AFM force spectroscopy. *Biochim. Biophys. Acta*, **1808**, 2646–2655.
73. Gorbenko, G. P. & Kinnunen, P. K. J. (2006). The role of lipid–protein interactions in amyloid-type protein fibril formation. *Chem. Phys. Lipids*, **141**, 72–82.
74. Reiss, A. B., Siller, K. A., Rahman, M. M., Chan, E. S. L., Ghiso, J. & de Leon, M. J. (2004). Cholesterol in neurologic disorders of the elderly: stroke and Alzheimer's disease. *Neurobiol. Aging*, **25**, 977–989.
75. Yu, X. & Zheng, J. (2012). Cholesterol promotes the interaction of Alzheimer β-amyloid monomer with lipid bilayer. *J. Mol. Biol.* **421**, 561–571.
76. van Echten-Deckert, G. & Walter, J. (2012). Sphingolipids: critical players in Alzheimer's disease. *Prog. Lipid Res.* **51**, 378–393.
77. McLaurin, J. & Chakrabartty, A. (1996). Membrane disruption by Alzheimer β-amyloid peptides mediated through specific finding to either phospholipids or gangliosides—implications for neurotoxicity. *J. Biol. Chem.* **271**, 26482–26489.
78. McLaurin, J. & Chakrabartty, A. (1997). Characterization of the interactions of Alzheimer beta-amyloid peptides with phospholipid membranes. *Eur. J. Biochem.* **245**, 355–363.
79. Sabate, R., Espargaro, A., Barbosa-Barros, L., Ventura, S. & Estelrich, J. (2012). Effect of the surface charge of artificial model membranes on the aggregation of amyloid β-peptide. *Biochimie*, **94**, 1730–1738.
80. Sabate, R., Gallardo, M. & Estelrich, J. (2005). Spontaneous incorporation of β-amyloid peptide into neutral liposomes. *Colloid Surf. A*, **270**, 13–17.
81. Kremer, J. J. & Murphy, R. M. (2003). Kinetics of adsorption of β-amyloid peptide A beta(1–40) to lipid bilayers. *J. Biochem. Biophys. Methods*, **57**, 159–169.
82. Lin, M.-S., Chiu, H.-M., Fan, F.-J., Tsai, H.-T., Wang, S. S. S., Chang, Y. & Chen, W.-Y. (2007). Kinetics and enthalpy measurements of interaction between β-amyloid and liposomes by surface plasmon resonance and isothermal titration microcalorimetry. *Colloid Surf. B*, **58**, 231–236.
83. Matsuzaki, K. & Horikiri, C. (1999). Interactions of amyloid β-peptide (1–40) with ganglioside-containing membranes. *Biochemistry*, **38**, 4137–4142.

84. Choo-Smith, L.-P. & Surewicz, W. K. (1997). Acceleration of amyloid fibril formation by specific binding of Aβ(1–40) peptide to ganglioside-containing membrane vesicles. *FEBS Lett.* **402**, 95–98.
85. Sciacca, M. F. M., Kotler, S. A., Brender, J. R., Chen, J., Lee, D. K. & Ramamoorthy, A. (2012). Two-step mechanism of membrane disruption by Aβ through membrane fragmentation and pore formation. *Biophys. J.* **103**, 702–710.
86. Martins, I. C., Kuperstein, I., Wilkinson, H., Maes, E., Vanbrabant, M., Jonckheere, W. *et al.* (2007). Lipids revert inert Aβ amyloid fibrils to neurotoxic protofibrils that affect learning in mice. *EMBO J.* **27**, 224–233.
87. Engel, M. F. M., VandenAkker, C. C., Schleeger, M., Velikov, K. P., Koenderink, G. H. & Bonn, M. (2012). The polyphenol EGCG inhibits amyloid formation less efficiently at phospholipid interfaces than in bulk solution. *J. Am. Chem. Soc.* **134**, 14781–14788.
88. Kremer, J. J., Pallitto, M. M., Sklansky, D. J. & Murphy, R. M. (2000). Correlation of β-amyloid aggregate size and hydrophobicity with decreased bilayer fluidity of model membranes. *Biochemistry*, **39**, 10309–10318.
89. Muller, W. E., Koch, S., Eckert, A., Hartmann, H. & Scheuer, K. (1995). Beta-amyloid peptide decreases membrane fluidity. *Brain Res.* **674**, 133–136.
90. Kim, D. H. & Frangos, J. A. (2008). Effects of amyloid β-peptides on the lysis tension of lipid bilayer vesicles containing oxysterols. *Biophys. J.* **95**, 620–628.
91. Morita, M., Vestergaard, M. d., Hamada, T. & Takagi, M. (2010). Real-time observation of model membrane dynamics induced by Alzheimer's amyloid beta. *Biophys. Chem.* **147**, 81–86.
92. Brender, J. R., Salamekh, S. & Ramamoorthy, A. (2012). Membrane disruption and early events in the aggregation of the diabetes related peptide IAPP from a molecular perspective. *Acc. Chem. Res.* **45**, 454–462.
93. Sciacca, M. F. M., Brender, J. R., Lee, D.-K. & Ramamoorthy, A. (2012). Phosphatidylethanolamine enhances amyloid fiber-dependent membrane fragmentation. *Biochemistry*, **51**, 7676–7684.
94. Smith, P. E. S., Brender, J. R. & Ramamoorthy, A. (2009). Induction of negative curvature as a mechanism of cell toxicity by amyloidogenic peptides: the case of islet amyloid polypeptide. *J. Am. Chem. Soc.* **131**, 4470–4478.
95. Zheng, F., Wu, Z. & Chen, Y. (2012). A quantitative method for the measurement of membrane affinity by polydiacetylene-based colorimetric assay. *Anal. Biochem.* **420**, 171–176.
96. Burke, K. A., Godbey, J. & Legleiter, J. (2011). Assessing mutant huntingtin fragment and polyglutamine aggregation by atomic force microscopy. *Methods*, **53**, 275–284.
97. Zhang, T. Y. & Suen, C. Y. (1984). A fast parallel algorithm for thinning digital patterns. *Commun. ACM*, **27**, 236–239.
98. Legleiter, J., Czilli, D. L., Gitter, B., DeMattos, R. B., Holtzman, D. M. & Kowalewski, T. (2004). Effect of different anti-Aβ antibodies on Aβ fibrillogenesis as assessed by atomic force microscopy. *J. Mol. Biol.* **335**, 997–1006.

Supplemental Material For:

Specific domains of Aβ facilitate aggregation on and association with lipid bilayers

Elizabeth A. Yates,[a] Sherry L. Owens,[a] Michael F. Lynch,[a] Elena M. Cucco,[b] C. Samuel Umbaugh,[a] and Justin Legleiter[a,b,c*]

[a]The C. Eugene Bennett Department of Chemistry, 217 Clark Hall, West Virginia University, Morgantown, WV, 26506, USA
[b]Center for Neuroscience, Robert C. Byrd Health Sciences Center, PO Box 9304, West Virginia University, Morgantown, WV, 26506, USA
[c]NanoSAFE, PO Box 6223, West Virginia University, Morgantown, WV, 26506, USA

[*]Corresponding author:
Justin Legleiter
The C. Eugene Bennett Department of Chemistry, 217 Clark Hall, West Virginia University, Morgantown, WV, 26506, USA
Phone: 304-293-0175
Email: justin.legleiter@mail.wvu.edu

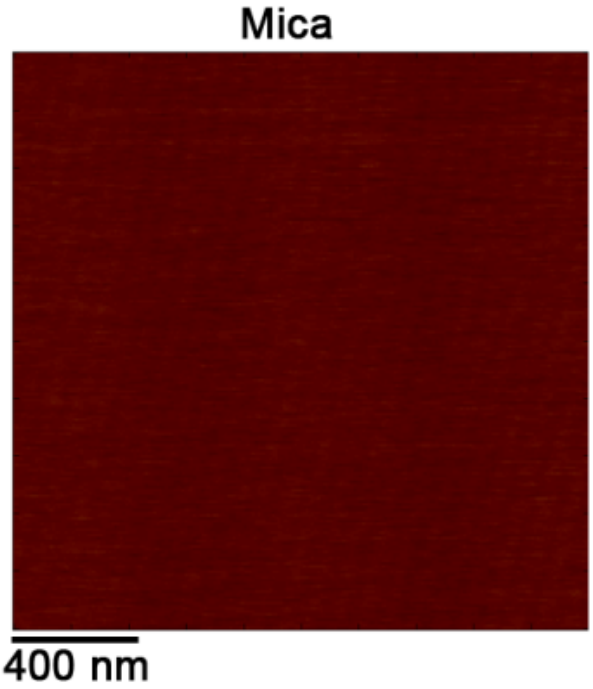

Supplemental Figure 1: Representative *in situ* tapping mode AFM image of a freshly cleaved mica surface in PBS buffer. The clean mica surface appears featureless.

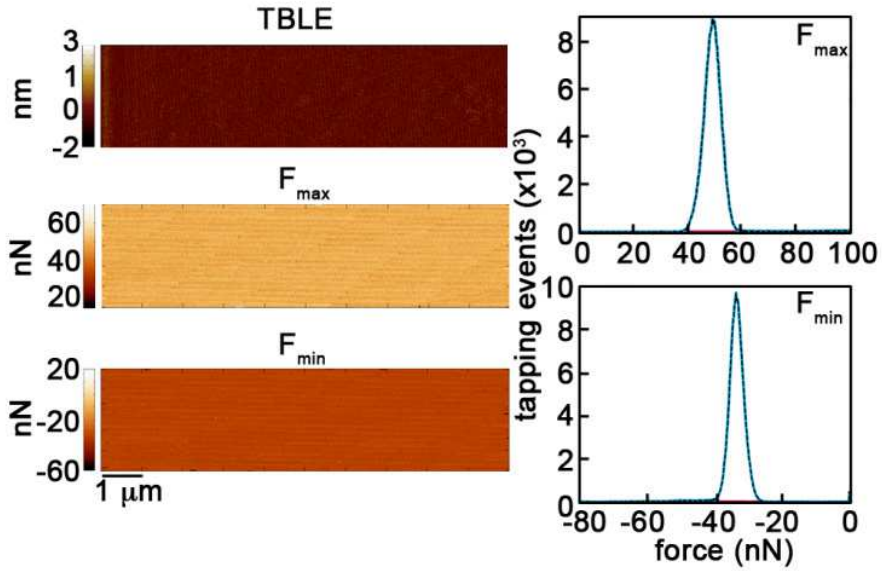

Supplemental Figure 2: Defect free TBLE bilayers have homogenous mechanical properties. AFM topography, F_{max}, and F_{min} images of TBLE bilayer were obtained using SPAM. Histograms of every tapping event (right of images) for F_{max} and F_{min} illustrate the unperturbed bilayer region.

Supplemental Table 1: Summary of the number of replicates and individual aggregates measured under different experimental conditions and assays

	$A\beta_{1-11}$	$A\beta_{1-28}$	$A\beta_{10-26}$	$A\beta_{12-24}$	$A\beta_{16-22}$	$A\beta_{22-35}$	$A\beta_{1-40}$
Aggregates formed under free solution conditions (ex situ AFM experiments)							
Images analyzed for oligomers	10	6	9	6	6	6	6
# of oligomers analyzed	1280	451	1363	2963	1034	279	693
Time points analyzed for oligomers	24-48h	24h	24-48h	24h	48h	24h	24h
Images analyzed for fibrils	7	9	9	5	3	12	5
# of fibrils analyzed	294	135	55	1806	1182	187	562
Time points analyzed for fibrils	72h	24-48h	24-48h	48h	72h	48h	24h
Replicates	3	7	3	3	7	7	7
Aggregates formed in the presence of TBLE bilayer (in situ AFM experiments)							
Images analyzed for oligomers	5	4	4	3	3	3	3
# of oligomers analyzed	104	300	1123	246	888	1028	491
Time points analyzed for oligomers	16-20h	16-20h	16-20h	16-20h	16-20h	16-20h	16-20h
Images analyzed for fibrils	n/a	n/a	3	n/a	4	4	3
# of fibrils analyzed	n/a	n/a	620	n/a	553	5477	2858
Time points analyzed for fibrils	n/a	n/a	16-20h	n/a	16-20h	16-20h	16-20h
Replicates	3	4	6	5	11	10	3
PDA Assay							
Replicates	3	3	3	3	3	3	3